PKHD1L1 is Required for Stereocilia Bundle Maintenance, Prolonged Hearing Function and Enhanced Resilience to Noise Exposure.

Olga S. Strelkova*, Richard T. Osgood*, Chunjie J. Tian*, Xinyuan Zhang, Evan Hale, Pedro De-la-Torre, Daniel M. Hathaway, Artur A. Indzhykulian**.

Department of Otolaryngology Head and Neck Surgery, Mass Eye and Ear, Harvard Medical School, Boston, MA, United States.

*These authors contributed equally to the study and are designated co-first authors.
** Correspondence should be addressed to inartur@hms.harvard.edu

Abstract

Sensory hair cells of the cochlea are essential for hearing, relying on the mechanosensitive stereocilia bundle at their apical pole for their function. Polycystic Kidney and Hepatic Disease 1-Like 1 (PKHD1L1) is a stereocilia protein required for normal hearing in mice, and for the formation of the transient stereocilia surface coat, expressed during early postnatal development. While the function of the stereocilia coat remains unclear, growing evidence supports PKHD1L1 as a human deafness gene. In this study we carry out in depth characterization of PKHD1L1 expression in mice during development and adulthood, analyze hair-cell bundle morphology and hearing function in aging PKHD1L1-defficient mouse lines, and assess their susceptibility to noise damage. Our findings reveal that PKHD1L1-deficient mice display no disruption to bundle cohesion or tectorial membrane attachment-crown formation during development. However, starting from 6 weeks of age, PKHD1L1-defficient mice display missing stereocilia and disruptions to bundle coherence. Both conditional and constitutive PKHD1L1 knock-out mice develop high-frequency hearing loss progressing to lower frequencies with age. Furthermore, PKHD1L1-deficient mice are susceptible to permanent hearing loss following low-level acoustic overexposure, which typically induces only temporary shifts in hearing thresholds. These results suggest a role for PKHD1L1 in establishing robust sensory hair bundles during development, necessary for maintaining bundle cohesion and function in response to acoustic trauma and aging.

Introduction

Auditory hair cells are highly specialized sensory cells located in the cochlea, essential for our sense of hearing by transducing the mechanical stimulus of sound into an electrical signal. Within the cochlea there are two types of hair cells: one row of inner hair cells (IHC), responsible for sound transduction; and three rows of electromotile outer hair cells (OHC), which amplify sound-evoked vibrations within the cochlea. Hair cells of the mammalian cochlea are terminally differentiated and do not regenerate once lost; therefore, hair-cell death or irreparable dysfunction leads to permanent sensorineural hearing loss.

Hair cells derive their name from the actin-rich stereocilia they carry at their apical poles, which collectively form the mechanosensitive sensory hair bundle. Hair bundles are composed of three rows of stereocilia arranged in a staircase pattern of ascending height. The mechanoelectrical-transducer (MET) machinery is located at the tips of the two shorter rows of stereocilia, linked to the adjacent taller row by fine protein filaments called tip links. Tip links mechanically gate the MET channels in response to bundle deflection, initiating the perception of sound and forming the basis of hearing (Beurg et al., 2009; Pickles et al., 1984). The tallest row of OHC stereocilia are embedded in the tectorial membrane (TM), a gelatinous extracellular matrix essential for hearing sensitivity and frequency selectivity (Legan et al., 2000, 2005; Sellon et al., 2019). The tips of the tallest row stereocilia are linked to the tectorial membrane by attachment crowns (Verpy et al., 2011). There are additional links between adjacent stereocilia, maintaining cohesion in the mature hair bundle. These inter-stereociliary links include horizontal top connectors in OHCs, and shaft connectors in IHCs (Goodyear et al., 2005; Nayak et al., 2007). During the establishment of the mature hair bundle in early postnatal development there is a rapidly changing array of additional, temporary, links on the surface of the stereocilia. Identified by electron microscopy, these include transient lateral links, ankle links, and OHC shaft connectors; in addition to a dense surface coat on the stereocilia and apical membrane of the cell, visualized by staining with tannic acid (Goodyear et al., 2005).

Following hair-cell gene expression analysis in mice, we previously identified Polycystic Kidney and Hepatic Disease 1-Like 1 (PKHD1L1), also known as fibrocystin like (Fibrocystin-L), as a component of the developmental stereocilia surface coat (Wu et al., 2019). PKHD1L1 is a large protein consisting of 4249 amino acids in mice and is highly enriched in hair cells. It is a membrane protein with a single-pass transmembrane domain; however, it is predominantly extracellular, with a very short 5-amino acid intracellular cytoplasmic domain at its C-terminal end. PKHD1L1 has been identified as a potential biomarker or has been implicated in several cancers, including but not limited to: thyroid cancer (Zheng et al., 2019), lung adenocarcinoma (Kang et al., 2023; L. Wang et al., 2023), renal cell carcinoma (Yang et al., 2023), skin cutaneous melanoma (Kang et al., 2023), cervical cancer (Zou et al., 2022), squamous cell carcinoma (Song et al., 2021), and breast cancer (Saravia et al., 2019). Furthermore, rare pathogenic variants of PKHD1L1 have been linked to conditions such as schizophrenia (Shang et al., 2024), in studies involving human subjects, and anxiety-like traits in rodents (Chitre et al., 2023).

We previously reported that PKHD1L1 localizes to the surface of stereocilia during early postnatal development. Using *Pkhd1l1*$^{fl/fl}$*::Atoh1-Cre*$^{+}$ mice, we established that it is required for the formation of the stereocilia surface coat, especially towards the tip of stereocilia (Wu et al., 2019). PKHD1L1-deficient mice showed no major morphological disruption to hair bundles at the onset of hearing; however, after initially exhibiting near-normal ABR and DPOAE thresholds, develop progressive hearing loss later in life (Wu et al., 2019). Similarly, auditory disruption has also been described in zebrafish deficient in PKHD1L1 (Makrogkikas et al., 2023). Double knockout of *pkhd1l1* zebrafish paralogs, *pkhd1l1α* and *pkhd1l1β,* reduces auditory-evoked startle responses in zebrafish at larvae stages, indicative of an early-onset hearing loss.

There is increasing evidence supporting *PKHD1L1* as a human deafness gene. We recently reported biallelic variants of *PKHD1L1* in four unrelated families with congenital non-syndromic sensorineural hearing loss (Redfield et al.). Reported PKHD1L1 variants were predicted to be damaging *in silico,* and some of the putative disease-causing mutations were shown to reduce the thermodynamic stabilities of PKHD1L1 protein fragments

in vitro (Redfield et al.). Furthermore, a large-scale exome study of 532 individuals recently identified the *PKHD1L1* gene as a possible contributor to hearing outcomes, with a higher variant load in older adults with hearing loss compared to the non-hearing loss group (Lewis et al., 2023).

The functions of the stereocilia coat, and specifically the role of PKHD1L1 on the surface of stereocilia during development, remain unclear. As the surface coat is only detected during the early postnatal development of cochlear hair cells, it has been suggested to play a role in bundle maturation (Goodyear et al., 2005). We previously hypothesized that PKHD1L1 could be required for the proper localization of other stereocilia components, essential for hair-cell function. Deficit in key stereocilia link proteins in mice often leads to morphological disruption of the hair bundle during development, resulting in profound hearing loss (reviewed by Petit and Richardson (Petit & Richardson, 2009)). However, the milder hearing loss phenotype previously observed in PKHD1L1-deficient mice more closely resembles those with tectorial membrane deficits (Goodyear et al., 2019; Verpy et al., 2008). Therefore, it has been suggested that PKHD1L1 may play a role in establishing connections between the OHC stereocilia with the tectorial membrane. However, an apparent disparity remains between the time of PKHD1L1 expression during development and the onset of observed phenotypic effects in PKHD1L1-deficient mice.

Hair-cell function is susceptible to disruption by genetic mutations and environmental factors such as noise exposure, ototoxic drug treatment, and aging. In the present study, we propose that PKHD1L1 is required for the establishment of robust sensory bundles, resilient to varied environmental stresses during aging. Experimentally, high noise levels have been shown to induce permanent shifts in hearing thresholds (PTS), while low-level acoustic overexposure leads to initial hearing threshold shifts which are then recovered over time, known as temporary threshold shifts (TTS) (Kujawa & Liberman, 2006; Ryan et al., 2016; Y. Wang et al., 2002). Administration of noise insult in an experimental setting therefore allow us to assess the sensitivity of PKHD1L1-deficient hair cells to environmental insult by determining whether threshold shifts induced by low-level acoustic overexposure are temporary or permanent.

In this study, we comprehensively characterize *Pkhd1l1* gene and protein expression during development and in adult mice. Morphological analysis in PKHD1L1-deficient mice revealed no developmental disruption to bundle cohesion or attachment-crown formation. However, progressive bundle disruption and missing stereocilia are observed in mice deficient in PKHD1L1 from 6 weeks of age onwards, with concurrent high frequency hearing loss progressing to lower frequencies with age in both conditional and constitutive *Pkhd1l1* knock-out mice. We find that PKHD1L1-deficient mice have a higher susceptibility to permanent hearing loss following low-level acoustic overexposure. Here, therefore, we demonstrate a role for PKHD1L1 in establishing robust sensory hair bundles during development, which is required in later life to maintain function in response to insult and aging.

Results

Pkhd1l1 mRNA is expressed in outer and inner hair cells during development.

Previously, we reported active transcription of *Pkhd1l1* in hair cells during early postnatal development (Wu et al., 2019). To investigate the discrepancy in the timeframe between the detection of PKHD1L1 protein and the physiological effects of its deletion on hearing function in later life, we first elected to directly, and more precisely, evaluate the *Pkhd1l1* mRNA levels within inner and outer hair cells during development and aging.

Using a commercially available probe targeting the 1061-2157 bp region (~8% of the 13049 bp transcript) of *Pkhd1l1* mRNA, we carried out *in-situ* hybridization by RNA scope in acutely dissected organ of Corti from P1 to 9-month-old mice. *Pkhd1l1* mRNA was visualized by fluorescence imaging in apical, middle, and basal turns of the cochlea. *Pkhd1l1* expression was observed as diffuse, as well as bright punctate labeling, in both IHCs and OHCs (Fig. 1a, and Sup. Fig. 1).

To quantify *Pkhd1l1* mRNA labeling intensity levels in individual cells, we utilized Cellpose, a deep-learning-based generalist algorithm for cellular segmentation (Stringer et al., 2021). Briefly, the DAPI stained hair cell nuclei were detected using Cellpose, and their ROIs transferred to imageJ for single cell intensity measurements of mRNA labeling in maximum intensity z-projections (Fig. 1b).

The intensity of mRNA labeling varied in an age- and cochlear region-dependent manner. Considering first, OHCs: *Pkhd1l1* mRNA fluorescence labeling intensity is highest in the basal region at P1 and drops rapidly during early postnatal development (Fig. 1a & c). Peak mRNA expression in the middle and apical regions occurs later, at P4 (Fig. 1c & Sup. Fig. 1a). As hair cells towards the base of the cochlea develop before those at the apex, and peak fluorescence intensity is similar between the regions, differences in mRNA expression between regions at a given time point are likely developmental rather than tonotopic. In all 3 regions, OHC *Pkhd1l1* mRNA fluorescence intensity drops to almost undetectable levels by P11 (comparable to negative control *dapB,* Sup. Fig.1b), before the onset of hearing (P21) and remains undetectable in mature hair cells at P24 and 9-month time points (Fig. 1 & Sup Fig. 1a).

Surprisingly, given that little PKHD1L1 was previously detected at the surface of IHCs at early postnatal time points (Wu et al., 2019), *Pkhd1l1* mRNA is also detected at comparatively high levels in inner hair cells. As with expression in OHCs, fluorescence intensity peaks first in early postnatal development (P7), although later than that observed in OHCs (P1-4). More curiously, however, *Pkhd1l1* mRNA is also detected at high levels in IHCs at the 9-month time point, (Fig. 1 & Sup. Fig. 1a) and not detected in negative control *dapB* (sup Fig.1b). These findings suggest a possibility of PKHD1L1 protein expression in IHCs in the adult cochlea.

PKHD1L1 is transiently expressed in cochlear hair cells during early postnatal development.

The abovementioned *Pkhd1l1* mRNA expression labeling results do not correlate well in timing or location with our previous findings of protein detection (Wu et al., 2019). Therefore, to more fully characterize the expression pattern of PKHD1L1, we carried out anti-PKHD1L1 immunofluorescence labeling in the cochlea throughout development and in adulthood (Fig. 2). Labeling was carried out in P4–9 month old *Pkhd1l1*$^{fl/fl}$*::Atoh1-Cre*$^{-}$ mice (Fig. 2 top 7 panels), facilitating the use of previously reported *Pkhd1l1*$^{fl/fl}$*::Atoh1-Cre*$^{+}$ mice as a negative labeling control (Fig. 2, bottom panel).

In agreement with our previous report, PKHD1L1 was detected in hair cells throughout the first postnatal week (Fig. 2 P4-P8) along the length of the cochlea (Sup. Fig. 2a). PKHD1L1 labeling was observed on the hair bundle stereocilia, with no specific signal detected in hair cell bodies (Sup Fig. 2c). Anti-PKHD1L1 labeling intensity gradually decreased with development, was largely gone by P10, and completely cleared in mature hair cells at P21.

153

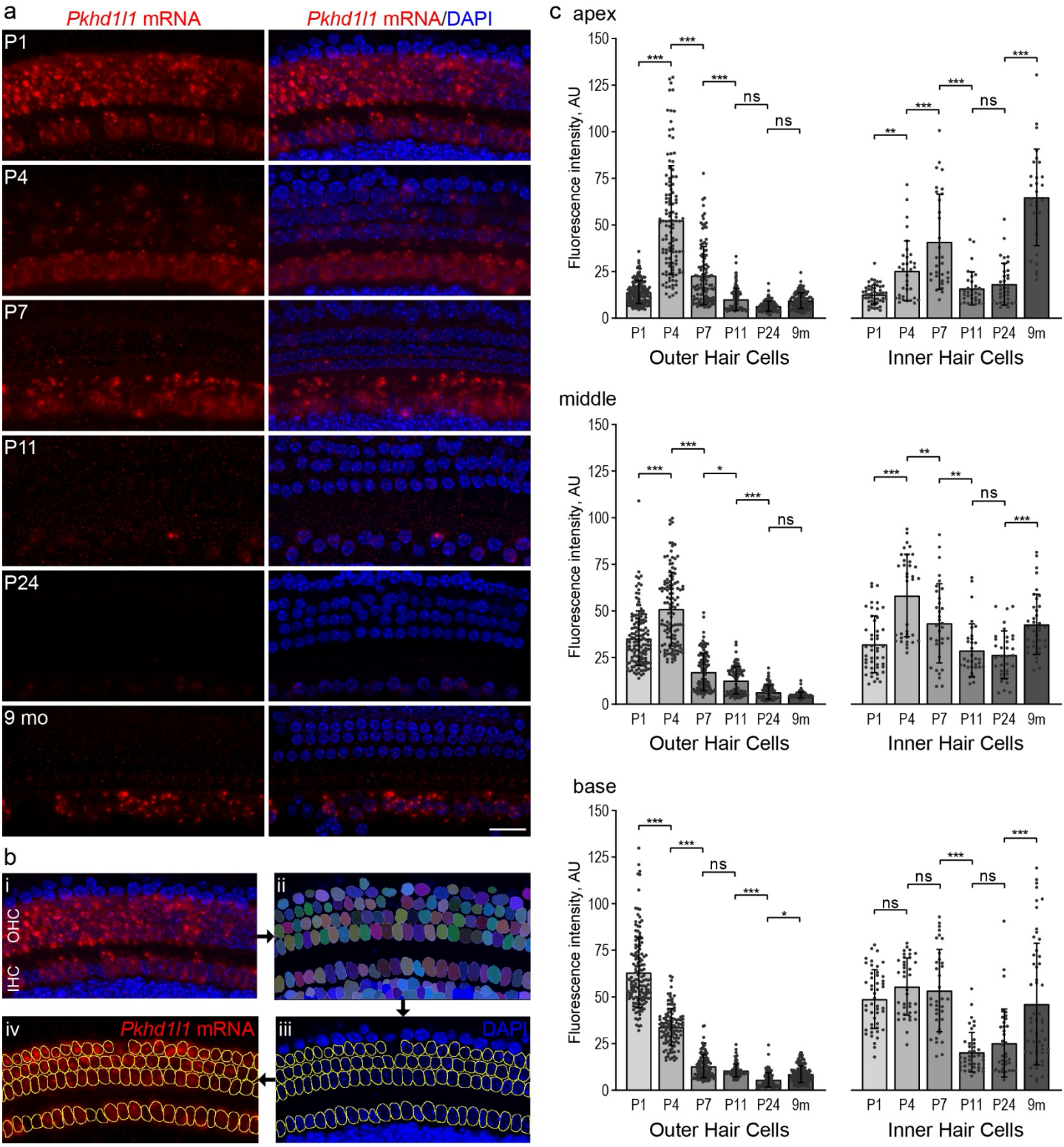

Figure 1. ***Pkhd1l1* mRNA levels in hair cells gradually decrease during early postnatal development**.
a, *In situ* detection of *Pkhd1l1* mRNA by RNAscope fluorescence labeling of the basal cochlear region. Maximum intensity z-projections. *Red, Pkhd1l1* mRNA fluorescence. *Blue*, DAPI. *Scale bar,* 20 µm. **b**, Schematic of RNAscope single cell fluorescence intensity quantification approach: nuclei in all cells were individually segmented using *Cellpose* analysis pipeline based on DAPI label, the masks representing hair-cell nuclei were assigned to IHCs or OHCs to measure *Pkhd1l1* mRNA fluorescence labeling intensity on a single-cell level. **c**, Average *Pkhd1l1* mRNA fluorescence intensity measurements in three cochlear locations from P1 to 9 months of age in OHCs *(left)* and IHCs *(right)*. *Pkhd1l1* mRNA levels in OHCs significantly decrease by P24 in all cochlear regions and remain virtually undetectable. *Pkhd1l1* mRNA levels in IHCs show a similar gradual downregulation during development, however, increase in the 9-months-old cochlea. Points represent individual cells; bars show mean ± SD. Two cochleae were analyzed per condition (15-80 cells from each). *Statistical analysis*, one-way ANOVA with Sidak's multiple comparison tests between adjacent time points, * $p<0.05$, ** $p<0.01$, *** $p<0.001$.

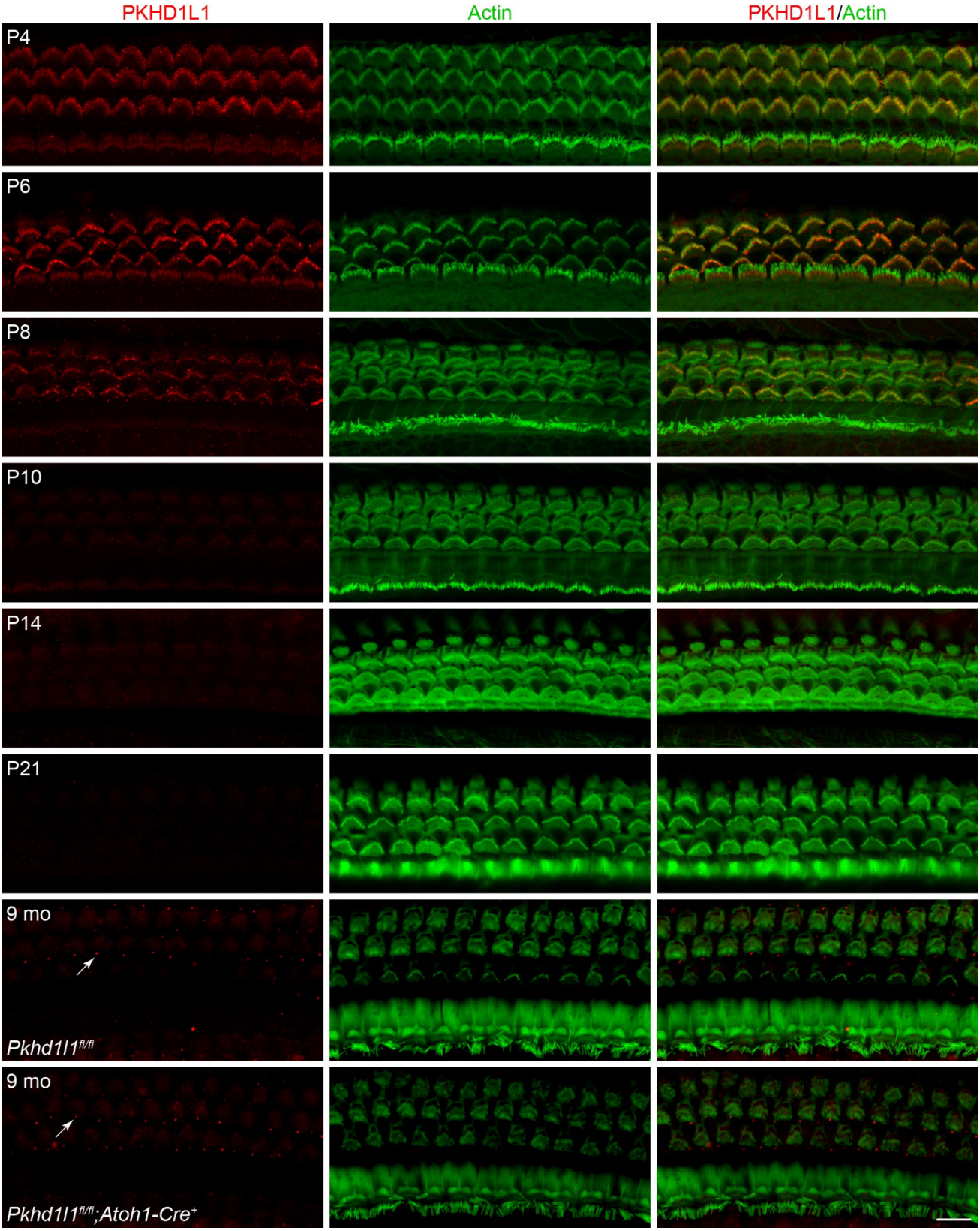

Figure 2. PKHD1L1 is only detected in hair cells during early postnatal development.
Anti-PKHD1L1 immunolabeling reports presence of PKHD1L1 protein in stereocilia bundles of early postnatal mice, with labeling intensity gradually decreasing by P10-P14. No specific anti-PKHD1L1 fluorescence labeling was observed in adult cochleae at 9 months, while some non-specific labeling is evident within basal bodies of kinocilia (white arrows). The *bottom* panel is from *Pkhd1l1*$^{fl/fl}$*::Atoh1-Cre*$^{+}$ mouse (negative control), while all other panels are from normal, *Pkhd1l1*$^{fl/fl}$*::Atoh1-Cre*$^{-}$ mice. *Red*, anti-PKHD1L1; *Green*, phalloidin labeling. Micrographs are maximum intensity z-projections of hair-cell apical poles and stereocilia bundles. Images are representative of >6 cochleae per time point. *Scale bar,* 10 µm.

155 Although PKHD1L1 is observed on inner hair cell bundles at P4 and P6, despite largely similar *Pkhd1l1* mRNA
156 expression results between IHCs and OHCs, protein labeling intensity was higher at the surface of the OHC
157 stereocilia bundles compared to IHCs (Fig. 2 compared to Fig. 1A). Furthermore, no anti-PKHD1L1
158 immunoreactivity was observed in IHC at 9 months. Fluorescence signal detected within the basal bodies of
159 kinocilia in *Pkhd1l1*$^{fl/fl}$*::Atoh1-Cre*$^{-}$ mice at this time point, is also found in *Pkhd1l1*$^{fl/fl}$*::Atoh1-Cre*$^{+}$ cochlea,
160 devoid of PKHD1L1, (Fig. 2 arrows, comparing bottom 2 panels) and is therefore concluded to be non-specific.
161 Similarly, no specific anti-PKHD1L1 immunolabeling signal was detected in the mouse utricle at P0 and P4
162 (data not shown).

163 From these data, we conclude there is not a direct correlation between in *Pkhd1l1* mRNA levels and protein
164 expression levels detected using immunolabeling techniques. PKHD1L1 protein expression labeling is
165 restricted to early postnatal development and localizes to the hair bundles of both IHCs and OHCs.

166

167 **PKHD1L1 expression is not redistributed on OHC hair bundle stereocilia during development.**

168 During early postnatal development, a transient surface coat, and several types of transient stereocilia links are
169 present on the developing stereocilia bundle (Goodyear et al., 2005). PKHD1L1 was previously demonstrated
170 to localize with the surface coat at P4 (Wu et al., 2019). Several key stereocilia components including the tip-
171 link proteins cadherin-23 (CDH23) (Michel et al., 2005) and protocadherin-15 (PCDH15) (Indzhykulian et al.,
172 2013; Kazmierczak et al., 2007); horizontal top connector and attachment crown protein stereocilin
173 (STRC)(Verpy et al., 2011); and transient ankle link component Vlgr1 (Goodyear & Richardson, 1999), have
174 been demonstrated to be spatially refined, concentrated, or redistributed, following their initially more diffuse
175 expression on the developing bundle. To determine the distribution pattern of PKHDIL1 on OHC bundles
176 during this developmental period, scanning electron microscopy (SEM) immunogold labeling of PKHD1L1 was
177 carried out on cochleae between P4 - P10 (Fig. 3).

178 Since EDTA decalcification is required for tissue dissection to enable immunogold SEM analysis in cochleae
179 older than P6, we first evaluated the effect of EDTA treatment on immunogold labeling efficiency. There was
180 no significant difference in the number of gold particles observed in P4 mouse cochleae, processed with and
181 without decalcification buffer (Sup. Fig. 3).

182 In agreement with immunofluorescence data (Fig 2), immunogold labeling on OHC bundles was observed
183 between P4–P10. Labeling is greatest at P4 with almost no labeling observed by P10 (Fig. 3). The average
184 number of gold particles per OHC stereocilium was 3.75 at P4, 1.8 at P6, 0.88 at P8 and 0.26 at P10 (Fig. 3c).
185 Very little gold labeling was detected in IHCs, unlike that observed in immunofluorescence (Fig. 3c compared
186 to Fig. 2.). This is likely as a result of reduced labeling efficiency by immunogold.

187 Upon close inspection of gold beads at the surface of stereocilia bundles, PKHD1L1 did not appear to localize
188 to any specific areas or links prior to the cessation of its expression at P10 (Fig. 3a). In agreement with
189 previously reported data at P4 (Wu et al., 2019), PKHD1L1 is found on all three stereocilia rows throughout
190 development. To evaluate the distribution of PKHD1L1 on specific stereocilia rows of OHC bundles during its
191 expression, we quantified the proportion of gold particles located on the tallest, middle and short stereocilia
192 rows at each time point (Fig. 3d,e). There is a slight increase in the proportion of gold beads located on the
193 tallest row, and decrease on the shortest row, between P4 and P6. However, this does not represent a
194 substantive change in the overall distribution of PKHD1L1 between the stereocilia rows. We therefore conclude
195 that PKHD1L1 is not spatially refined or redistributed on the surface of OHC hair bundles during development.

196
197

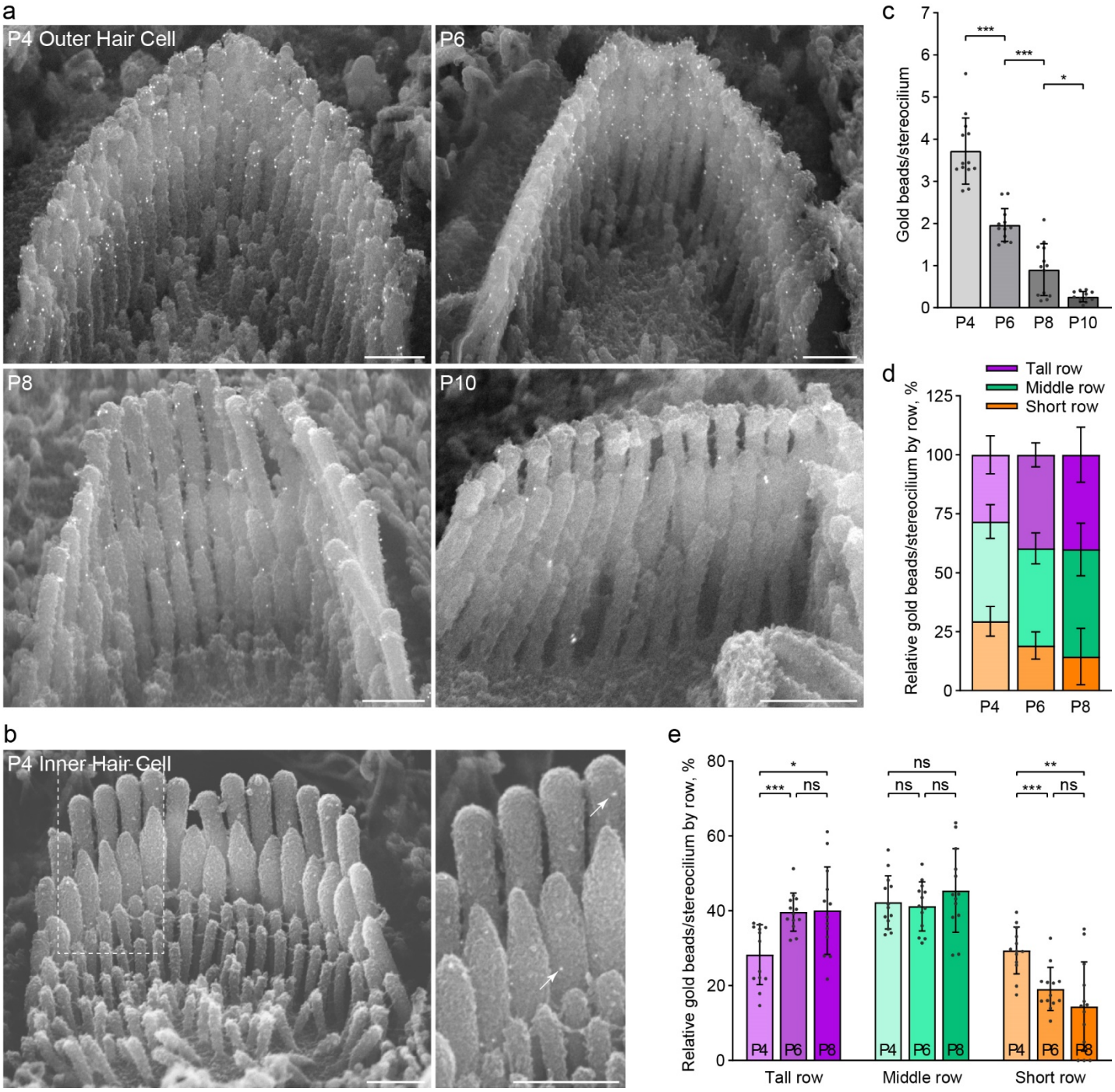

198

Figure 3. The distribution of anti-PKHD1L1 immunogold labels on the surface of OHC bundles does not change during development. a, Anti-PKHD1L1 immunogold SEM of OHC bundles in the mid/basal region at P4, P6, P8 and P10. **b**, P4 IHC bundles are labeled with fewer gold beads (arrows), as compared to OHCs. *Scale bars,* 500 nm. **c**, Quantification of the total number of gold beads per OHC stereocilium show a gradual decrease of labeling density, with most of the labeling gone by P10. *Statistical analysis*, one-way ANOVA with Sidak's multiple comparison tests between consecutive time points. **d**, **e,** Distribution of gold beads at the surface of the tallest, middle, and short rows of stereocilia as a portion of the total number of gold beads per bundle, normalized per stereocilium. A slight increase in the proportion of gold beads in the tallest row, and a reduction in the proportion of gold beads in the shortest row, is observed between P4 and P6. *Statistical analysis*, two-way ANOVA with matched design between stereocilia rows from the same cell. Tukey's multiple comparison tests are shown between time points for each row. * $p<0.05$, ** $p<0.01$, *** $p<0.001$. All results are presented as mean ± SD, datapoints represent individual cells (n=13 at each time point).

Tectorial membrane attachment crowns and imprints retain normal morphology in PKHD1L1-deficient mice.

The progressive hearing loss phenotype we previously observed in PKHD1L1-deficient mice (Wu et al., 2019) is similar to that observed in mice with tectorial membrane deficits, such as in STRC and CEACAM16-deficient mice (Goodyear et al., 2019; Verpy et al., 2008). Interaction with the tectorial membrane, established during early postnatal development, is critical for OHC function. We therefore sought to investigate the establishment, and maintenance of OHC attachment with the tectorial membrane in PKHD1L1-deficient mice as a possible source of pathology.

STRC plays a key role in attachment crown formation between OHC tall row stereocilia and tectorial membrane (Verpy et al., 2011). We detected STRC at the tips of stereocilia in *Pkhd1l1*$^{fl/fl}$*::Atoh1-Cre*$^{+}$ mice, as in *Pkhd1l1*$^{fl/fl}$ littermate controls, by immunofluorescence at P35 – a time point when bundles and the tectorial membrane are fully developed (Fig. 4a,b). Immunogold SEM of bundles demonstrates the correct localization of STRC, primarily in halos around the tip of the tallest stereocilia, in addition to between stereocilia tips, in both PKHD1L1 deficient mice and littermate controls (Fig. 4c). We therefore conclude that PKHD1L1 is not required for the localization of STRC to attachment crowns or horizontal top connectors. Furthermore, OHC bundle imprints in the tectorial membrane, observed by SEM, still form in PKHD1L1-defficient mice, and were still present after 6 months (Fig. 4d). Together these data suggest that the establishment OHC links with the TM are not disrupted in PKHD1L1-defficient mice.

Loss of PKHD1L1 induces late onset progressive hearing loss and stereocilia disorganization.

Despite the restricted temporal expression PKHD1L1 to early postnatal development, our previous study revealed progressive hearing loss in *Pkhd1l1* deficient mice. However, no gross morphological changes were found during adolescence (Wu et al., 2019). We sought to verify hearing loss in *Pkhd1l1*$^{fl/fl}$*::Atoh1-Cre*$^{+}$ conditional hair-cell-specific knock out (cKO) and constitutive *Pkhd1l*$^{-/-}$ KO mice, in addition to conducting comprehensive stereocilia analysis by SEM in PKHD1L1-deficient mice during aging.

The *Atoh1-Cre*$^{+}$ line expresses Cre as early as embryonic day 10.5. In juveniles Cre expression, and in turn *Pkhd1l1* KO in *Pkhd1l1*$^{fl/fl}$*::Atoh1-Cre*$^{+}$ mice, is limited to sensory hair cells, as well as some supporting cells and cochlear and vestibular sensory neurons (Matei et al., 2005). Hearing deficit was observed by ABR recordings in cKO *Pkhd1l1*$^{fl/fl}$*::Atoh1-Cre*$^{+}$ mice compared to *Pkhd1l1*$^{fl/fl}$ (Cre^{-}) littermates (Fig. 5a). ABR thresholds were elevated at 6 weeks in the high-frequency region (32 kHz, 45 kHz), progressing to lower-frequency regions (16 kHz, 22 kHz) by 9 months of age. Consistent with the predominant localization of PKHD1L1 to OHC bundles, hearing deficits were mirrored in DPOAE thresholds. Thresholds were elevated first at 32 kHz at 6 weeks, progressing in severity and frequency range by 9 months (Fig. 5a), indicative of progressive OHC dysfunction.

The use of hair-cell-specific *Pkhd1l1* KO in *Pkhd1l1*$^{fl/fl}$*::Atoh1-Cre*$^{+}$ mice is advantageous to mitigate against phenotypes related to possible unknown developmental or central processing functions of PKHD1L1 in other tissues and cell types. However, elevated ABR thresholds have been reported in mice with hair cells expressing Cre (Matern et al., 2017). In order to confirm that hearing deficit was not as a result of Cre expression, we generated constitutive KO *Pkhd1l*$^{-/-}$ mice. Constitutive KO of PKHD1L1 was not embryonically lethal; *Pkhd1l*$^{-/-}$ mice appear to develop normally and breed well. Elevated ABR and DPOAE thresholds were found in *Pkhd1l*$^{-/-}$ mice from 12 weeks, comparable to those observed in *Pkhd1l1*$^{fl/fl}$*::Atoh1-Cre*$^{+}$ mice, again progressing to lower frequencies with age (Sup. Fig. 4). These data confirm progressive hearing deficits as a result of PKHD1L1 KO.

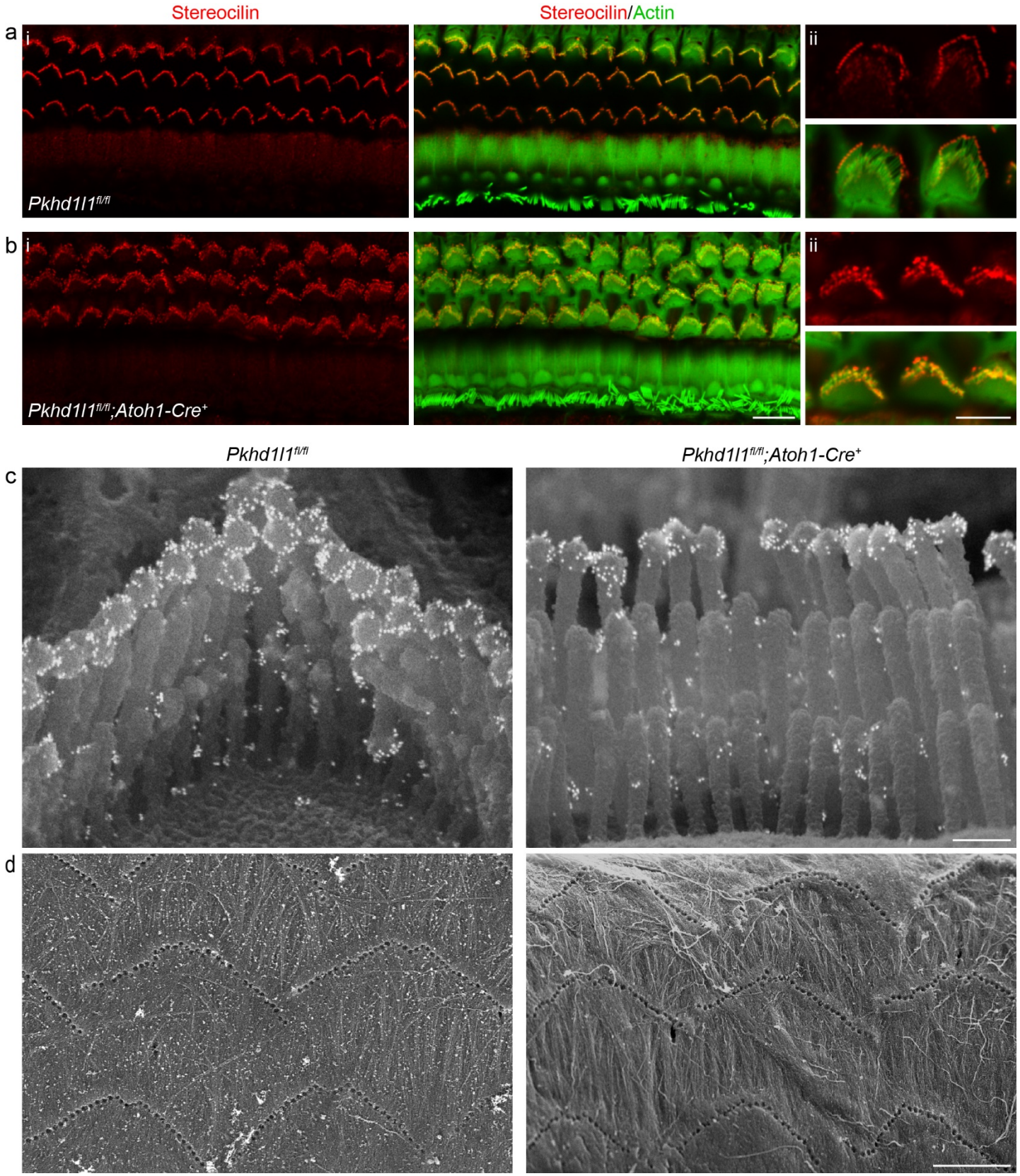

Figure 4. Stereocilin is properly localized to the OHC stereocilia bundles in PKHD1L1-deficient mice.
Anti-STRC immunofluorescence labeling of OHCs in the basal region of P35 mouse cochlea localizes to the tips of stereocilia (**a**) *Pkhd1l1*$^{fl/fl}$*::Atoh1-Cre*$^{-}$ controls and (**b**) *Pkhd1l1*$^{fl/fl}$*::Atoh1-Cre*$^{+}$ mice (ii, inset with higher magnification). *Red*, anti-PKHD1L1; *Green*, phalloidin labeling. Images are representative of 2 cochleae per genotype. **c,** Anti-STRC immunogold SEM of OHC stereocilia in *Pkhd1l1*$^{fl/fl}$*::Atoh1-Cre*$^{+}$ and their *Pkhd1l1*$^{fl/fl}$*::Atoh1-Cre*$^{-}$ control mice at P29. The gold bead labels form a well-characterized ring pattern at the tips of tall row stereocilia in control and PKHD1L1-deficient mice. Images are representative of 2 cochleae per genotype. **d,** SEM imaging of TM reveal normal imprints in 6-month-old *Pkhd1l1*$^{fl/fl}$*::Atoh1-Cre*$^{+}$ mice and *Pkhd1l1*$^{fl/fl}$*::Atoh1-Cre*$^{-}$ controls. Images are representative of 3 cochleae per genotype. *Scale bars*, *a-b* i, 10 μm; ii, 5 μm; *c*, 250 nm; *d,* 5 μm.

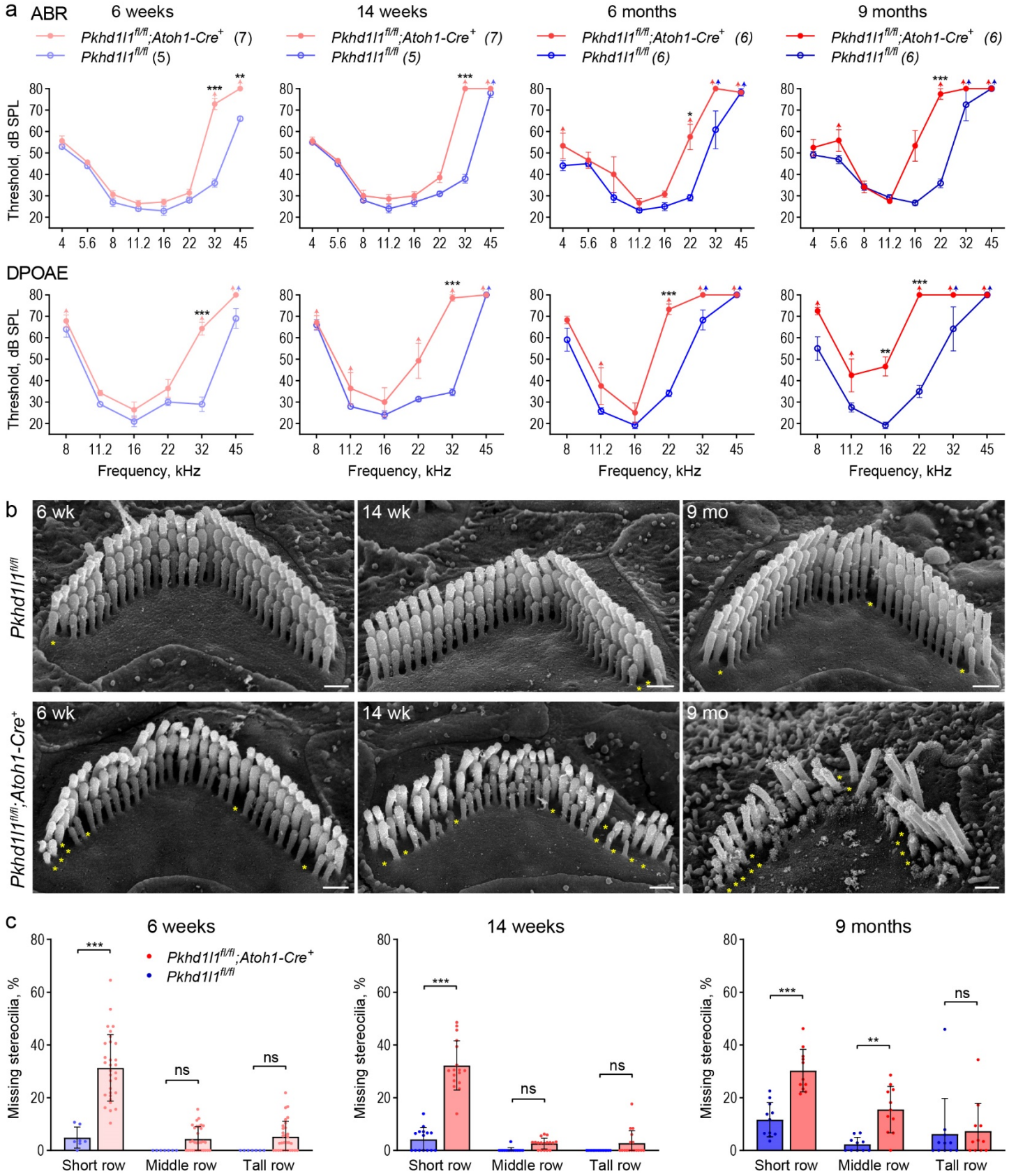

Figure 5. PKHD1L1-deficient mice display progressive hearing loss and stereocilia disruption.
a, ABR and DPOAE of *Pkhd1l1*$^{fl/fl}$*::Atoh1-Cre*$^{+}$ and *Pkhd1l1*$^{fl/fl}$*::Atoh1-Cre*$^{-}$ mice show progressive high-frequency hearing loss in PKHD1L1-deficient mice as early as 6 weeks. Data are shown as mean ± SEM. Up-arrows indicate that at the highest SPL level tested (80 dB SPL), at least one mouse in the group had no detectable thresholds at that frequency. *Statistical analysis*, two-way ANOVA with matched design between frequencies from the same mouse. Sidak's multiple comparison tests are shown between genotypes for each frequency. **b**, SEM of OHC stereocilia bundles at 6 weeks, 14 weeks, and 9 months in the basal region (32 kHz) reveal progressive stereocilia loss (asterisks) and bundle disorganization. *Scale bars*, 500 nm. **c**, Quantification of missing stereocilia in OHC bundles in the basal turn (32 kHz region) of the cochlea, presented as percentage of stereocilia missing per row. There is a greater stereocilia loss in *Pkhd1l1*$^{fl/fl}$*::Atoh1-Cre*$^{+}$ mice as compared to their *Pkhd1l1*$^{fl/fl}$*::Atoh1-Cre*$^{-}$ littermates at all age points. Data displayed as mean ± SD, points represent individual cells (see n in *Methods*). *Statistical analysis*, two-way ANOVA with matched design between rows from the same cell. Sidak's multiple comparison tests are shown between rows for each genotype. *p<0.05, **p<0.01, ***p<0.001.

The morphology of OHC stereocilia bundles was examined using SEM in *Pkhd1l1*$^{fl/fl}$*::Atoh1-Cre*$^{+}$ cKO hair cells during the progression of hearing deficit (Fig. 5b). Mild stereocilia loss (Fig. 5b, yellow asterisks) was observed after 6 weeks, becoming more pronounced over time. To analyze the progression of the stereocilia loss from OHCs as aging occurs, we calculated the number of missing stereocilia from each row of the bundle. Notably, stereocilia loss was most significant in the shortest row, progressing to the taller rows with age; most prominently in, but not limited to, the high frequency basal region (Fig. 5c - 32 kHz region, Sup. Fig. 5 - 22 and 16 kHz regions).

Hair cell stereocilia bundles of *Pkhd1l1*$^{fl/fl}$*::Atoh1-Cre*$^{+}$ cKO mice at 6 weeks of age show no overt signs of disrupted development or disorganization, as compared to *Pkhd1l1*$^{fl/fl}$ controls (Fig. 5b). However, bundle disorganization is observed at 14 weeks increasing in severity by 9 months of age. OHC bundle structure was well maintained in *Pkhd1l1*$^{fl/fl}$ littermate controls, with rare instances of stereocilia loss. These data implicate a role for PKHD1L1 expression during development in the maintenance and potential stabilization of stereocilia bundles, and in turn OHC function, in later life.

Acoustic overexposure leads to permanent hearing loss in PKHD1L1-dificent mice.

Low-level noise trauma paradigms have been shown to induce temporary threshold shifts (TTS) in hearing function, which are subsequently recovered to normal levels (Jensen et al., 2015; Y. Wang et al., 2002). Despite the expression of PKHD1L1 being restricted to early postnatal development, PKHD1L1-deficient mice display delayed onset progressive phenotypes in ABRs, DPOAEs and OHC bundle morphologies (Fig. 5 & Sup. Fig. 4). This could be indicative of a protein required for the establishment of more durable hair bundle morphology and function. To test this hypothesis, we assayed bundle and hearing heath and durability following noise overexposure.

Exposure to 94 dB SPL 8-16 kHz bandpass noise for 2 hours was carried out at 6 weeks of age in *Pkhd1l*$^{fl/fl}$*::Atoh1-Cre*$^{+}$ mice and *Pkhd1l1*$^{fl/fl}$ littermate controls – a time point and frequency at which there is not normally any hearing deficit in *Pkhd1l1*$^{fl/fl}$*::Atoh1-Cre*$^{+}$ mice (Fig. 5a). Higher noise levels were initially trailed in wild type mice, however these lead to permanent threshold shifts (PTS), and therefore considered too damaging for BL6 background mice to recover from.

ABRs and DPOAEs were measured at 1 day, 2 days, 2 weeks, and 8 weeks, after noise exposure and compared to baseline levels collected prior to the noise protocol, in order to determine threshold shifts resulting from the noise exposure (Fig. 6a). In both *Pkhd1l1*$^{fl/fl}$ and *Pkhd1l1*$^{fl/fl}$*::Atoh1-Cre*$^{+}$ mice ABR and DPOAE thresholds were elevated in the 16-32 kHz region 1 day post noise exposure with some recovery after 2 days (Fig. 6b). Thresholds were back to baseline levels by 2 weeks post noise exposure in *Pkhd1l1*$^{fl/fl}$ mice, consistent with TTS. Thresholds did not return to baseline levels in *Pkhd1l1*$^{fl/fl}$*::Atoh1-Cre*$^{+}$ mice however, with threshold shifts maintained at 2 and 8 weeks following noise insult (Fig. 6b).

In the absence of noise trauma (Sup. Fig. 6) threshold shifts of <10 dB were observed at high frequencies between the 6-week evaluation time point and an additional 8-week 'recovery' time point in both genotypes, as a result of aging in these mice. This does not however account for the large, pan-frequency, threshold shifts observed in PKHD1L1 deficient mice alone following noise exposure. These data therefore show the noise exposure, normally only sufficient to cause TTS in normal mice, leads to PTS in PKHD1L1-deficient mice.

We examined OHC bundle morphology in *Pkhd1l1*$^{fl/fl}$*::Atoh1-Cre*$^{+}$ mice and *Pkhd1l1*$^{fl/fl}$ littermates 2 and 8 weeks following noise exposure, time points at which TTS were recovered in control mice but not PKHD1L1-defficent mice (Fig. 7). In control *Pkhd1l1*$^{fl/fl}$ mice, bundles remained intact and well-organized at 2 and 8 weeks post-noise exposure. In contrast, in *Pkhd1l1*$^{fl/fl}$*::Atoh1-Cre*$^{+}$ mice, bundle disorganization was observed 2 weeks following noise exposure (Fig. 7a), particularly in tallest row stereocilia, in addition to some loss of short

row stereocilia, as expected at this age in PKHD1L1-defficient mice (comparison to Fig. 5b). By 8 weeks post-noise exposure, bundles were further disrupted, with instances of tall row stereocilia loss and disorganization (Fig. 7b). These findings demonstrate that PKHD1L1 deficiency during development increases susceptibility to bundle disruption during low-level noise exposure, leading to permanent threshold shifts.

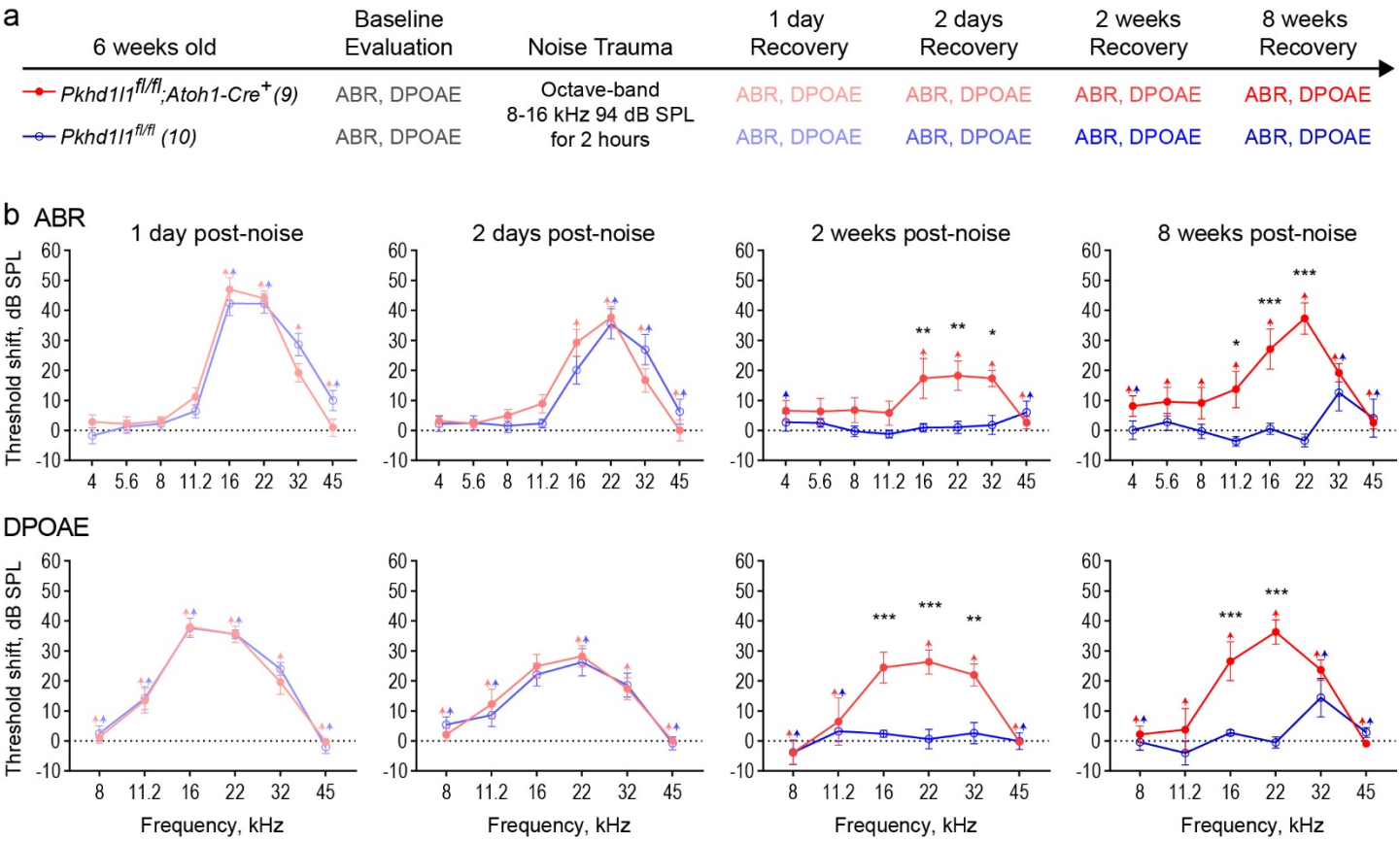

Figure 6. PKHD1L1-deficient mice experience permanent hearing loss after noise trauma levels that induce TTS in control animals. **a**, Experimental design. 6-week-old *Pkhd1l1*$^{fl/fl}$*::Atoh1-Cre*$^{+}$ mice and *Pkhd1l1*$^{fl/fl}$*::Atoh1-Cre*$^{-}$ control animals had baseline ABR and DPOAE evaluation prior to TTS-inducing level of noise trauma (8-16 kHz, 94 dB SPL). ABR and DPOAEs were subsequently recorded at 1 day, 2 days, 2 weeks, and 8 weeks, post noise exposure. **b**, ABR and DPOAE threshold shifts from pre-noise baseline evaluation. *Pkhd1l1*$^{fl/fl}$*::Atoh1-Cre*$^{-}$ control mice (*blue*) exhibit temporary threshold shifts in ABRs and DPOAEs followed by recovery to baseline levels 2 weeks post-noise trauma, while *Pkhd1l1*$^{fl/fl}$*::Atoh1-Cre*$^{+}$ mice (*red*) show only slight recovery 2 days after noise trauma, and permanent threshold shift in ABRs and DPOAEs at later time points. Data are shown as mean ± SEM. Up-arrows indicate that at the highest SPL level tested, at least one mouse in the group had no detectable thresholds at that frequency prior to calculation of threshold shift. *Statistical analysis*, two-way ANOVA with matched design between frequencies from the same mouse. Sidak's multiple comparison tests are shown between genotypes for each frequency. *p<0.05, **p<0.01, ***p<0.001.

295

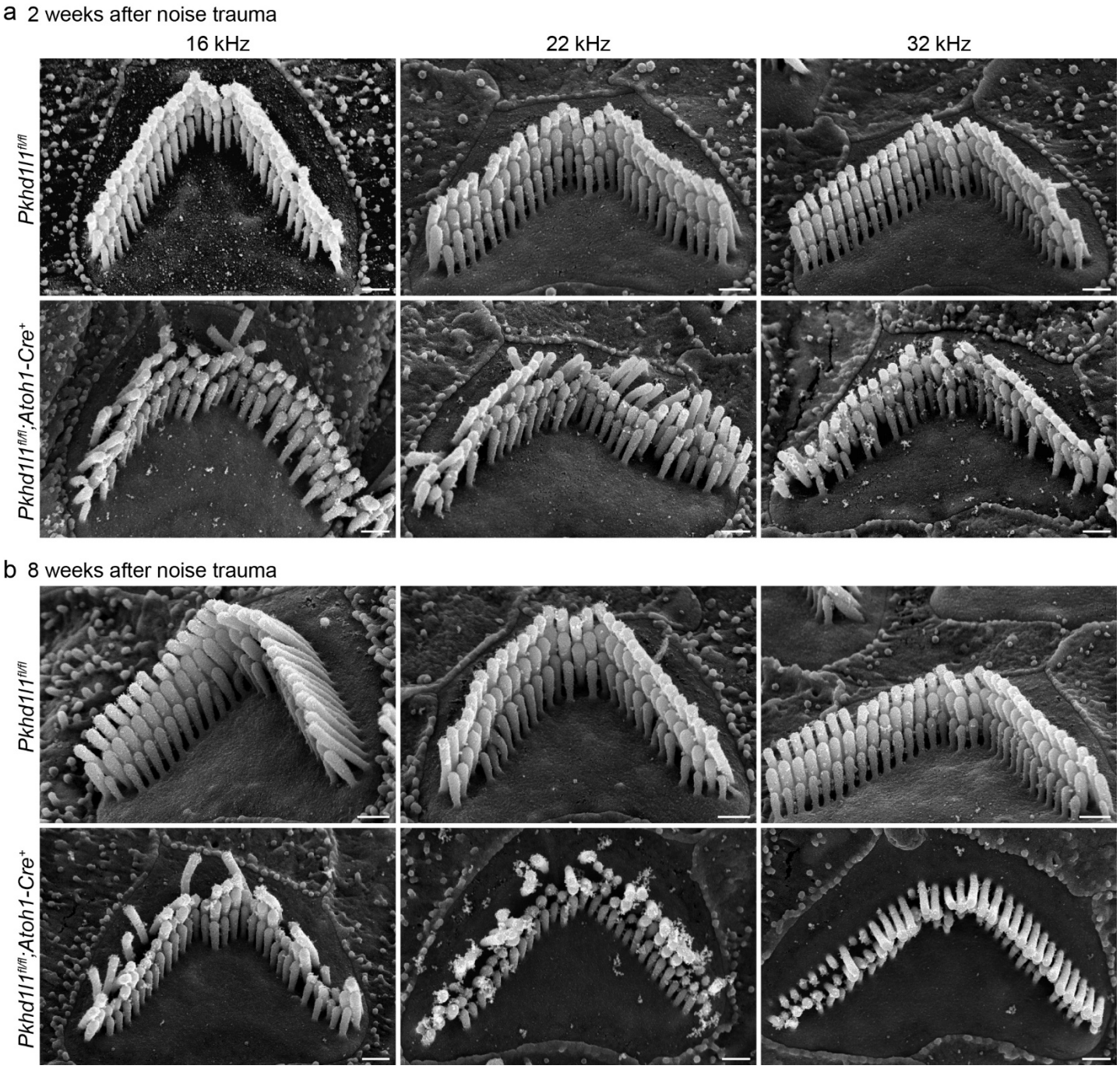

Figure 7. PKHD1L1-deficient mice exhibit stereocilia loss and bundle disorganization following low-level noise trauma. SEM of OHCs following TTS-level noise trauma. **a,** 2 weeks after noise exposure *Pkhd1l1*$^{fl/fl}$*::Atoh1-Cre*$^{+}$ bundle morphology is disrupted in comparison with *Pkhd1l1*$^{fl/fl}$*::Atoh1-Cre*$^{-}$ littermate controls, also exposed to noise. **b,** 8 weeks after noise trauma stereocilia bundles in *Pkhd1l1*$^{fl/fl}$*::Atoh1-Cre*$^{+}$ mice are further disrupted with instances of missing and shortened tall row stereocilia. *Scale bar*, 500 nm.

Discussion

In this study we aim to better understand the role of PKHD1L1 in the sensory hair bundle and hearing. In order to address the previously observed (Wu et al., 2019) disparity between the early expression of *Pkhd1l1* and the later onset of phenotypic defect in PKHD1L1-deficient mice, we first fully characterized *Pkhd1l1* gene and protein expression during development and in adult mice. We confirmed developmentally restricted expression of PKHD1L1 on the sensory hair bundles of inner and outer hair cells. We further demonstrated by immunogold SEM that PKHD1L1 does not localize or redistribute to specific stereocilia bundle structures during this developmental period.

Contrary to our previous findings (Wu et al., 2019), we observe progressive bundle disruption and missing stereocilia in mice deficient in PKHD1L1 from 6 weeks of age onwards. We report hearing threshold shifts, initially restricted to high frequencies, subsequently progressing to lower frequencies, in both conditional hair-cell specific and constitutive *Pkhd1l1* KO-out mice. Finally, we show that PKHD1L1 deficient mice have an increased susceptibility to permanent hearing loss following low-level acoustic overexposure, implicating the expression of PKHD1L1 during development in the establishment of stable bundles that are robust to environmental insult in later life.

PKHD1L1 expression, localization, and potential cleavage.

PKHD1L1 protein was detected during the first 10 days of postnatal hair bundle development, primarily localized on the stereocilia of OHC, with some expression observed in IHC (Fig. 2&3, and Sup. Fig. 2). Gene expression analysis using RNA scope revealed corresponding early-postnatal *Pkhd1l1* gene expression. However, unexpectedly, transcription of *Pkhd1l1* signal was also observed in the IHCs of 9-month-old adult mice (Fig. 1) despite no corresponding protein detection (Fig. 2). This discrepancy suggests that PKHD1L1 protein detection could be absent due to lack of mRNA translation in IHC at this time point, or that the translated protein was not detectable at the IHC stereocilia by immunolabeling.

In silico analysis reveals that PKHD1L1 is predicted to have a very short cytoplasmic domain, consisting of only 5 amino acids, and is inserted into the plasma membrane by a single transmembrane domain. However, it predominantly extends extracellularly, spanning a significant length of 4202 amino acids (Fig. 8 models C-terminal residues p.3011-p.4249). In our previous study we demonstrated that PKHD1L1 labeling (by antibody NBP2-13765, also used in this study, with epitope amino acids p.3670-p.3739 Fig. 8a lime) is sensitive to the protease subtilisin (Wu et al., 2019). Additionally, PKHD1L1 has been identified in the 'sheddome' of activated blood platelets by mass spectrometry (Fong et al., 2011). The authors reported that the presence of PKHD1L1 following activation was substantially reduced by inhibitors of the protease ADAM17. These reports suggest that PKHD1L1 is susceptible to proteolytic cleavage *in vitro* and *in vivo*.

To reconcile our findings of *Pkhd1l1* mRNA expression in adult cochlea with the lack of antibody labeling of the PKHD1L1 protein, we carried out cleavage site prediction on the protein sequence of *Pkhd1l1* orthologs from 10 species (Sup. Table 1). Using the ProP 1.0 online prediction tool (Duckert et al., 2004), we identified three potential cleavage sites in the PKHD1L1 sequence (numbered based upon the mouse sequence): p.R3566, p.R3976, and p.R3986 (Sup. Fig. 7).

We utilized Alphafold2 to model the structure of a PKHD1L1 fragment and mapped the potential cleavage sites (Fig. 8a-c). Site 1 (p.R3566), with a confidence score below threshold in mice but present in other species, is located in a parallel beta-helix repeat (PbH1) rich region with structural homology to the human TMEM2 protein ectodomain (Fig. 8a & b). While site 2 (p.R3976), not identified in other species, and with a confidence score below threshold, and site 3 (p.R2986, with the highest confidence score in all species) are located within a domain with structural homology to the PCDH15 MAD12 domain (Fig. 8a & c). Notably, cleavage site 3 is highly conserved across 10 different orthologs and lies within an exposed loop of PKHD1L1 MAD-like domain (Fig. 8d). Proteolytic cleavage at site 3 would release an extracellular protein fragment containing the NBP2-

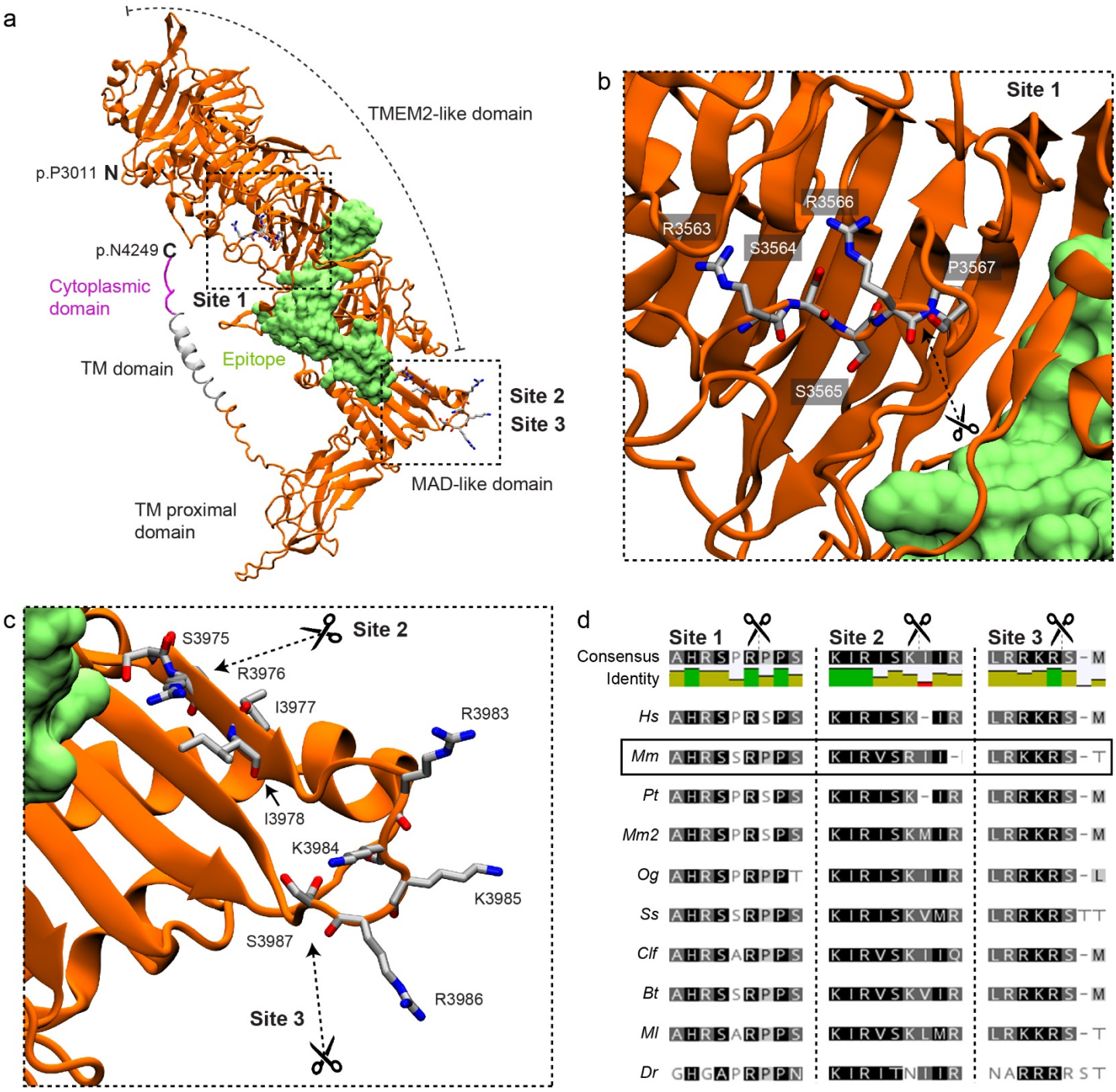

Figure 8. PKHD1L1 contains potential proteolytic cleavage sites.
a, AlphaFold2 modelling was used to predict the structure of a *Mm* PKHD1L1 protein fragment comprising the residues p.P3011-4249. Residue numbering includes the signal peptide (20 amino acids) using the reference sequence NP_619615.2. The protein fragment is depicted in cartoon representation of the ectodomain fragment (orange), transmembrane domain (grey) and cytoplasmic domain (pink). The epitope for the anti-PKHD1L1 antibodies used in this study (NBP2-13765 —against p.3670-p.3739) is depicted in surface representation (lime). Potential cleavage sites at p.R3566 (site 1), p.R3976 (site 2), and p.R3986 (site 3) are depicted with scissors. The antibody epitope region and the transmembrane domain are separated by the PKHD1L1 MAD-like domain with predicted cleavage sites 2 and 3, suggesting that labeling of the PKHD1L1 ectodomain might be absent following PKHD1L1 cleavage *in vivo*. **b, c,** Insets representing zoomed-in views of the putative cleavage sites. **d**, Protein sequence alignment of the predicted PKHD1L1 cleavage site regions across 10 different species (see accession codes in Sup. Table 1). Analysis was carried out with the Geneious software. Background colors represent the rate of residue conservation: black indicates high-sequence similarity, while white indicates poor residue similarity or its absence. A consensus sequence is shown for all the species at the top of the panel, with a color -coded identity map to illustrate the level of consensus between the different species. Images were rendered with the VMD software.

13765 antibody epitope, thus hindering the labeling of the remaining membrane-tethered portion of the PKHD1L1 peptide by the NBP2-13765 antibody used for immunolabeling in this study. This analysis suggests that protein cleavage could explain the discrepancy in *Pkhd1l1* mRNA detection and protein labeling in the inner hair cells of 9-month-old mice. Although we did not observe PKHD1L1 labeling on the tectorial membrane of young mice (P6-P10, data not shown), further investigation is warranted to determine whether PKHD1L1 is cleaved *in vivo* in adult mice, and to explore the potential role of the cleaved PKHD1L1 fragment.

The role of PKHD1L1 and the stereocilia coat.

The function of the stereocilia coat during bundle maturation in early-postnatal development remains unclear. Although often considered together, distinct from the developmentally transient surface coat labeled with tannic acid, the stereocilia and apical surface of hair cells are covered by a glycocalyx coat, which can be visualized by cationic dyes such as Alcian blue (Santi & Anderson, 1987). This glycocalyx coat persists in mature hair cells, and has been suggested to contribute to bundle cohesion during stimulation and/or preventing stereocilia fusion (Dolgobrodov et al., 2000a, 2000b; Karavitaki & Corey, 2010). However, PKHD1L1 expression is limited to early-postnatal development (Fig. 2 & 3) and is primarily localized to the external face of the stereocilia rather than between them (Wu et al., 2019), suggesting a distinct role.

Deficits in key mechanotransduction machinery or stereocilia link proteins often cause morphological disruption of the hair bundle during development, resulting in a profound hearing loss (Richardson & Petit, 2019). In contrast, PKHD1L1-deficient mice undergo normal bundle maturation (Fig. 2 & 3), and exhibit only high-frequency hearing loss at younger ages (Fig. 5 & Sup. Fig. 4). This indicates that PKHD1L1 expression during development is likely not essential for the gross maturation of the hair bundle, or the localization and function of the MET complex.

We previously proposed that PKHD1L1 may play a role in establishing connection between the OHC stereocilia with the tectorial membrane. The late-onset mild hearing loss phenotype, and increased DPOAE thresholds, observed in PKHD1L1-deficient mice is similar to that of tectorial membrane deficits previously reported in CEACAM16-deficient mice (Goodyear et al., 2019). Furthermore, PKHD1L1 is primarily located on OHC, towards the tips of the stereocilia (Fig. 3)(Wu et al., 2019), where TM attachment crowns form. However, attachment crowns only form on the tallest row stereocilia, and unlike previously reported for key TM attachment crown protein stereocilin (Verpy et al., 2011), here we see no major redistribution or refinement in the localization of PKHD1L1 to the tallest row of stereocilia during its expression period (Fig. 3). Moreover, we observed largely normal localization of stereocilin in PKHD1L1-defficient mice (Fig. 4).

Unlike in mice deficient in attachment crown proteins stereocilin, otogelin, otogelin-like or tubby (Avan et al., 2019; Han et al., 2020), in which attachment crown formation is disrupted, stereocilia imprints are still present in the tectorial membrane of PKHD1L1-defficient mice (Fig. 4d). However, as TM imprints formed during development are likely permanent (Morisaki et al., 1991), this does not preclude the possibility of TM attachments weakening in PKHD1L1-defficient mice as they age and/or are exposed to noise insult. This could lead to a progressive detachment of the tectorial membrane from tall row stereocilia later in the animal's life. Unfortunately, it is extremely challenging to experimentally detect such slowly progressing changes of TM attachment to stereocilia. After normal initial development, minor, but progressive, disruption to the coherence of hair bundles is observed in mice deficient in PKHD1L1 (Fig. 5b). Similar minor disruptions to bundle coherence are observed at earlier time points in attachment crown protein mutants (Avan et al., 2019; Han et al., 2020). However, stereocilia loss is also observed in PKHD1L1-deficient mice, initially primarily in short row stereocilia (Fig. 5b & c). This phenotype is unlikely to be caused by disruption of tall row stereocilia attachment to the TM.

Curiously, following acoustic overexposure, stereocilia loss and disorganization in PHD1L1-deficient mice was observed in tall row stereocilia (Fig. 7), suggestive of TM involvement. However, tall row damage after noise exposure in PKHD1L1 deficient mice could result from either aberrant interaction between the stereocilia and

390 tectorial membrane, or an inability of the bundle to cope with the potential increased strain on the stereocilia
391 from the tectorial membrane during noise trauma. Intriguingly in the *Tubby* mutant *tub/tub;Map1a*^{AKR}, (deficient
392 in the attachment crown and horizontal top connector component TUB, combined with the restorative *Map1a*
393 polymorphism on an AKR/N background) attachment crowns are present in the absence of horizontal top
394 connectors. These mice display normal DPOAEs, however also display increased sensitivity to noise damage
395 (Han et al., 2020). While this alone does not account for the phenotypes observed in PKHD1L1 deficient mice,
396 the proximity of PKHD1L1 during its expression to link structures, and the similarities in the deficits observed in
397 their disruption, maintain interaction with stereocilia links and the tectorial membrane as an appealing
398 molecular mechanism of action for PKHD1L1.

399

400 **PKHD1L1 is required for the formation of robust stereocilia bundles in noise trauma and aging.**

401 Knock out of PKHD1L1 leads to adult-onset hearing loss, OHC dysfunction, and stereocilia loss, which
402 progress with age (Fig. 5). Low-level acoustic overexposure has been demonstrated to induce temporary shifts
403 in hearing thresholds, which can be reversed following a 2-week recovery period (Wang et al., 2002). Upon
404 recovery, normal mice exhibit no disruption to hair bundle morphology (observed Fig. 7 *Pkhd1l1*$^{fl/fl}$ controls),
405 however, TTS-levels of acoustic overexposure can induce other lasting neuronal pathologies outside the scope
406 of this study (Fernandez et al., 2020; Kujawa & Liberman, 2009). In the absence of PKHD1L1, threshold shifts
407 in response to low-level noise insult are not reversed, concurrent with morphological disruption of stereocilia
408 bundles (Fig. 6 & 7). We therefore propose that PKHD1L1 expression during early postnatal bundle maturation
409 is required for the establishment of robust sensory bundles, less susceptible to damage and disruption in
410 response to noise exposure and aging.

411 We previously reported elevated high frequency ABR and DPOAE thresholds in *Pkhd1l1*$^{fl/fl}$*::Atoh1-Cre*$^{+}$ mice as
412 early as 3 weeks of age, progressing across all tested frequencies by 6 months (Wu et al., 2019). In the
413 present study we again report progressive hearing loss, initially at high frequencies, however, elevations in
414 ABR and DPOAE thresholds were less pronounced and progressed to lower frequencies more slowly than
415 observed previously (Fig. 5). We further verified these findings by generating and evaluating the hearing
416 function in constitutive *Pkhd1l*$^{-/-}$ KO mice, in which a similar phenotype is observed (Sup. Fig. 4).

417 The recordings from these studies were carried out in different institutions, however in both instances
418 PKHD1L1-defficient mice were compared to littermate controls. As we have determined that PKHD1L1-
419 defficient bundles are more susceptible to noise-induced damage, the variability in the acoustic environment
420 between the animal facilities experienced by PKHD1L1-defficient mice used in these studies may account for
421 the differences seen in hearing thresholds. Interestingly, audiogram profiles of human patients with non-
422 syndromic hearing loss and biallelic PKHD1L1 variants were also diverse (Redfield et al.). As PKHD1L1
423 variants may make hair cells more vulnerable to damage due to environmental factors, it is likely that in
424 addition to the potential differences in the damaging effect of distinct PKHD1L1 variants at the protein level,
425 hearing loss profiles in affected probands may also reflect differing levels of acoustic exposure throughout their
426 lives.

427 With increasing evidence to support PKHD1L1 as a human deafness gene (Lewis et al., 2023; Redfield et al.),
428 it is apparent that the function of PKHD1L1 requires further study. Unfortunately, the role of the developmental
429 stereocilia coat remains unclear. Although PKHD1L1 does not localize to any known link structures during its
430 expression period, PKHD1L1 has many protein binding domains. Identification of PKHD1L1's binding partners
431 would enable the identification of further coat proteins and provide a better understanding of the role of the
432 stereocilia coat during bundle maturation and function. Finally, we also highlight the possibility of PKHD1L1
433 ectodomain shedding by hair cells during development.

434 In conclusion, although the specific molecular function of PKHD1L1 remains elusive, in the present study we
435 build on our current understanding of the role of PKHD1L1 in hearing and deafness. After comprehensive

436 characterization of *Pkhd1l1* gene and protein expression during development and in adult mice, we find
437 PKHD1L1 protein expression on the stereocilia bundle is restricted to early postnatal development. PKHD1L1-
438 deficient mice display no disruption to bundle cohesion or tectorial membrane attachment-crown formation
439 during development. However, progressive bundle disruption and missing stereocilia are later observed in mice
440 deficient in PKHD1L1, with concurrent delayed onset progressive hearing loss. Furthermore, we show that
441 PKHD1L1-deficient mice are susceptible to permanent hearing loss following acoustic overexposure, which
442 typically induces only temporary shifts in hearing thresholds. Here therefore, we propose that PKHD1L1
443 expression is necessary for the establishment of robust sensory bundles that are required for prolonged
444 hearing function and resilience to noise exposure.

Materials and Methods

Generation of Knockout Mice.

We transferred *Pkhd1l1*$^{fl/fl}$*::Atoh1-Cre*$^{+}$ mice from Corey Lab at Harvard Medical School to Mass Eye and Ear Animal Care Facility. These mice exhibit PKHD1L1 deficiency selectively in hair cells, triggered by Cre recombinase expression driven by the *Atoh1* promotor. As previously reported (Wu et al., 2019), the *Pkhd1l1*$^{fl/fl}$ allele contains 2 loxP sites flanking exon 10, encoding the beginning of IPT2 domain of PKHD1L1. Upon *Atoh1* expression in hair cells, Cre recombinase deletes exon 10 (71 bp), leading to a frameshift and a premature stop codon downstream of the excised region (Wu et al., 2019). The resulting PKHD1L1 peptide is 258 amino acids (including signal peptide), and consists of a single non-membrane-bound IPT domain.

To generate a constitutive KO model, *Pkhd1l1*$^{fl/fl}$ mice were crossed with an EIIa-Cre mouse line (The Jackson Laboratory, B6.FVB-Tg(EIIa-cre)C5379Lmgd/J, #003724) to delete exon 10 from germline. Once homozygous *Pkhd1l1*$^{-/-}$ alleles were established, the EIIa-Cre allele was bred out of the colony. Genomic PCR implemented the following primer pairs: Pkhd1l1fl-F (TGA CAC AAC ATA CTG AGC AT) and Pkhd1l1fl-R (GGA AAC TCC TGT TGA AAC AA), yielding a 624 bp fl band and 438 bp WT band; Pkhd1l1KO-F (TGACACAACATACTGAGCAT) and Pkhd1l1KO-R (TTTGAAGACCACACTGAGAG), yielding a 422 bp KO band and 828 bp WT band; EIIA-Cre-F (ATTTGCCTGCATTACCGGTC) and EIIa-Cre-R (ATCAACGTTTTCTTTTCGGA), yielding a 349 bp Cre band.

All procedures were conducted in compliance with ethical regulations approved by the Institutional Animal Care and Use Committee of Mass Eye and Ear.

Immunofluorescence Labeling.

Cochleae were dissected in L-15 medium, fixed in 4% formaldehyde (EMS, #15713) in HBSS for 1 hour and washed with Ca^{2+}, Mg^{2+}-free HBSS. For mice older than P6, fixed cochleae were decalcified in 0.12M EDTA (pH=7.0) for 2 days, washed, then micro-dissected, and permeabilized in 0.5% Triton X-100 (Thermo scientific, #85111) in Ca^{2+}, Mg^{2+}-free HBSS for 30 minutes. Samples were blocked with 10% goat serum (Jackson ImmunoResearch, #005-000-121) in 0.5% Triton X-100 on Ca^{2+}, Mg^{2+}-free HBSS for 1 hour and incubated in 1:200, rabbit anti-PKHD1L1 (Novus Bio #NBP2-13765) overnight at 4℃. Samples were washed with Ca^{2+}, Mg^{2+}-free HBSS and stained for 2 hours in 1:500, Goat anti-Rabbit CF568 (Biotium #20099) and phalloidin CF488 (1:20, Biotium #00042) in the blocking solution. Stereocilin protein labeling was carried out as previously described (Ref Han et. Al., 2022). Anti-STRC antibody (used 1:50) was kindly provided by Dr. Jinwoong Bok, and previously validated in their study (Han et al., 2020). Following washes, samples were mounted on slides with the Prolong Diamond antifade kit (ThermoFisherScientific # P36961) and imaged on a Leica SP8 confocal microscope using a 63x 1.3NA objective lens.

RNAscope *in-situ* hybridization labeling and analysis.

The RNA labeling procedure was carried out as previously described (Ghosh et al., 2022). Mouse temporal bones were fixed in 4% PFA at room temperature for 3 hours. Cochleae were dissected and the organs of Corti were then placed in cold RNAlater solution in a 96 round bottom well plate and stored at 4°C. Samples were dehydrated by a series of 50, 70, 95, and 100% ethanol washes, each for 5 minutes. Hereafter, each step was followed by washes with milli-Q water. Samples were immersed in 3% H_2O_2 (RNAscope® Hydrogen Peroxide, ACD) for 30 minutes at room temperature, incubated in low-pH antigen unmasking solution (Citrate-Based, Vector Laboratories) at 65°C (HybEZII oven, ACD) twice, and incubated in protease plus (RNAscope® Protease Plus, ACD) for 30 minutes at room temperature. Samples were then left in water in 4°C overnight. A custom-ordered *Pkhd1l1* probe (mRNA region 1061-2157bp; exons 12-19) as well as positive and negative control probes were obtained from ACD and applied to samples for 2-hours of hybridization at 40°C. Signals

were amplified using the RNAscope 2.5 HD Detection Reagents - RED (warmed to room temperature). AMP1-4 were conducted at 40°C, while AMP 5-6 at room temperature. The duration for AMP1-6 was 30, 15, 30, 15, 25, and 10 minutes respectively, each step followed by 3 low pH antigen unmasking solution washes for 5 minutes each. After amplification, a RED-A and B cocktail at a ratio of 75:1 (shielded from UV light) was applied to the samples for 10 minutes at room temperature, then washed in water extensively. Samples were stained with DAPI (1:2000 dilution in Ca^{2+}, Mg^{2+}-free HBSS) for 5 minutes and mounted on slides using Prolong Diamond mountant and imaged with a Leica SP8 confocal microscope with a 63x 1.3 NA objective lens.

Images were processed with ImageJ as maximum intensity projections and analyzed using Cellpose (Stringer et al., 2021)to generate a cell mask for each nucleus based on DAPI labeling. Next, resulting ROIs outlining individual cells were transferred to ImageJ. All ROIs corresponding to IHCs and OHCs were used to measure the average intensity values per pixel within each ROI, while the cell masks representing other cells were discarded. Independently, to validate these results, the images were also analyzed manually in ImageJ by outlining 9-12 OHCs or 3-4 IHCs and resulting ROIs were used for average intensity measurements. As there were no substantial differences between Cellpose-generated ROI intensity measurements using the nuclear stain signal, and similar results obtained by manual ROI assignment encompassing entire hair cell bodies, automated and unbiased Cellpose mask generation was favored. Data were plotted and analyzed in GraphPad Prism.

Scanning Electron Microscopy.

Mouse cochleae were fixed with 2.5% glutaraldehyde in 0.1 M cacodylate buffer (EMS, #15960) supplemented with 2 mM $CaCl_2$ for 1.5-2 hours at room temperature, then washed in distilled water (DW). The bony capsule was carefully drilled away with a diamond micro-drill (Ideal Micro Drill, #67-1200A). The organ of Corti was revealed by removing the lateral wall, and the tectorial membrane was removed. For some cochleae the tectorial membranes were also saved and processed for SEM imaging to assess stereocilia imprints.

Samples were rinsed with 0.1 M sodium cacodylate buffer, then stained with 1% Osmium tetroxide(O) (EMS, #19152O) for 1 hour, followed by the treatment with 1% saturated thiocarbohydrazide(T) diluted in DW for 30 minutes. These treatments were repeated, with 3 × 10 min DW washes between steps, using an alternating O-T-O-T-O sequence. Samples were dehydrated in a series of ethanol washes and critical point dried from liquid CO_2 (Tousimis Autosamdri 815). Next, samples were mounted on aluminum specimen stubs with carbon tape and sputter-coated with 3.0 nm of platinum (Leica EM ACE600) and imaged with a Hitachi S-4700 FE-SEM.

Quantification of missing stereocilia.

The number of missing stereocilia was manually quantified from SEM images in three cochlear regions. Data were plotted and analyzed in GraphPad Prism. The number of hair cells from which quantification was carried out in each region per genotype is listed in the table below (Table 1) (*Pkhd1l1*$^{fl/fl}$*::Atoh1-Cre*$^{+}$ mice are listed as *Cre*$^{+}$, *Pkhd1l1*$^{fl/fl}$ mice are listed as *Cre*$^{-}$*)*:

Table 1. Number of hair cells used for quantification of stereocilia loss.

	6 weeks old		**14 weeks old**		**9 months old**	
	***Cre*$^{+}$**	***Cre*$^{-}$**	***Cre*$^{+}$**	***Cre*$^{-}$**	***Cre*$^{+}$**	***Cre*$^{-}$**
16 kHz	18	11	6	2	7	5
22 kHz	32	9	12	15	12	12
32 kHz	32	7	17	15	11	11

527 **Immunogold SEM and image analysis.**

528 The labeling was carried out as previously described (Ivanchenko et al., 2021). Cochleae from P4, P6, P8 and
529 P10 mice were dissected in L-15 medium, fixed in 4% formaldehyde (PFA, EMS, #15713) in HBSS for 1 hour,
530 then washed with Ca^{2+}, Mg^{2+} free HBSS. Samples from mice older than P4 were decalcified in 0.12M EDTA
531 (pH=7.0) for 2 days after fixation prior to micro-dissection. Samples were incubated for 1 hour in blocking
532 solution containing 10% goat serum (Jackson ImmunoResearch, #005-000-121) diluted in Ca^{2+}, Mg^{2+}-free
533 HBSS, then stained overnight at 4°C in 1:200 rabbit anti-PKHD1L1, (Novus Bio #NBP2-13765) in blocking
534 solution. Samples were washed in Ca^{2+}, Mg^{2+} free HBSS and incubated in 12 nm Gold AffiniPure Goat anti-
535 Rabbit secondary antibody (1:30 Jackson ImmunoResearch #111-205-144) overnight at 4°C. After washing
536 steps, samples were post-fixed with 2.5% glutaraldehyde in 0.1 M sodium cacodylate buffer (pH 7.2, EMS,
537 #15960) supplemented with 2 mM $CaCl_2$ for 1 hour, then washed with distilled water. Samples were
538 dehydrated, critical point dried and mounted as mentioned above. Dried samples were sputter-coated with
539 Palladium (~4.0 nm) and imaged with Hitachi S-4700 FE-SEM or FEI Helios 660 using insertable backscatter
540 detectors. The number of gold beads per each row of stereocilia was quantified manually. For every age point,
541 13 stereocilia bundles were analyzed. Data were plotted and analyzed in GraphPad Prism.

542

543 **ABR and DPOAE recordings.**

544 ABR and DPOAE thresholds were measured using an EPL Acoustic system in an acoustically and electrically
545 shielded soundproof chamber, as described previously (Kujawa & Liberman, 2009). Mice were anesthetized
546 via intraperitoneal injection of 100 mg/kg ketamine and 10 mg/kg xylazine. Artificial tears were applied to
547 protect the animal's eyes. The outer ear canals were exposed and the tympanic membranes were examined to
548 ensure normal appearance before calibrated earphone placement. Three subdermal needle electrodes were
549 inserted between the ears (reference), behind the pinna (recording), and near the tail (ground). Upon
550 completion, anesthetized animals were placed on a 37°C heating pad for recovery.

551 Tone-pip ABR stimuli spanned 4-45 kHz, each had a 5 ms duration, 0.5 ms rise-fall time, and of an alternating
552 polarity at 30 Hz. For each pure tone frequency tested, the sound pressure level (SPL) ranged from 20-80 dB.
553 Responses were amplified (10,000x), filtered (0.3-3 kHz), and averaged (512x) by the Cochlear Function Test
554 Suite. To determine thresholds were analyzed using the ABR Peak Analysis software (Eaton-Peabody
555 Laboratories(Suthakar & Liberman, 2019)). ABR thresholds were determined by the lowest SPL at which a
556 recurring 5-peak waveform was observed.

557 DPOAEs were detected in response to 2 simultaneous pure tones, f1 and f2 (f2/f1 = 1.2; f2 spanned 4-45 kHz
558 in half-octave steps and 10-80 dB SPL in 5 dB increments) with the level ratio L1=L2+10. The algorithm to
559 determine the DPOAE threshold for each frequency was an estimate of the crossing point of two curves, 2f1-f2
560 (dB) and 2f1-f2Nse (dB). No distinction was made between a precisely 80 dB threshold and one that was
561 above the testing limit. All data were plotted and analyzed in GraphPad Prism.

562

563 **Low-level acoustic overexposure.**

564 Following baseline ABR and DPOAE analysis (carried out as described above), awake 6-week-old mice were
565 held unrestrained in small cages and exposed to an octave-band noise (8–16 kHz) for 2 hours at 94 dB SPL,
566 which is identified as the highest non-neuropathic noise level associated with temporary threshold shifts
567 (Jensen et al., 2015), referred to hear as low-level acoustic overexposure. Sound exposure was created by a
568 white-noise source, filtered, amplified, and delivered through a horn attached to the top of the exposure booth.
569 Exposure levels were measured in each cage with a 0.25 inch Brüel and Kjær condenser microphone. ABR
570 and DPOAEs were measured 1 day, 2 days, 2 weeks, and 8 weeks after noise exposure. Thresholds were
571 averaged from the analysis of 2 independent researchers. Threshold shifts from baseline were calculated for

572 each mouse at each frequency and time point. Control mice received no noise exposure. All data were plotted
573 and analyzed in GraphPad Prism.

574

575 **Protein sequence analysis and prediction of PKHD1L1 cleavage sites.**

576 To predict potential cleavage sites in the PKHD1L1 protein sequence, we compared 10 different PKHD1L1
577 ortholog sequences extracted from the National Center for Biotechnology Information (NCBI) protein database
578 (Sup. Table S1). Species were chosen based on sequence availability and taxonomical diversity. To analyze
579 the complete sequences, each was split into two protein fragments with < 4,000 amino acids and uploaded into
580 the ProP 1.0. online server tool (Duckert et al., 2004). In Sup. Figure 7 the cleavage site prediction for the
581 Human PKHD1L1 is showed comprising the residue p.R3012 to its C-terminal ending residue. The equivalent
582 protein fragments were selected after protein sequence alignment for the other 9 orthologs (See Sup. Table S1
583 for NCBI residue numbering including signal peptides). Cleavage sites were predicted using the ProP 1.0.
584 default values. This online tool predicts arginine (R) and lysine (K) pro-peptide cleavage sites using an
585 ensemble of neural networks. Scores of > 0.5 indicate that the residue is predicted to be followed by a pro-
586 peptide cleavage site. The higher the score the more confident the prediction.

587 For sequence identity analysis of the PKHD1L1 cleavage site regions sequences were aligned with the
588 ClustalW algorithm (Larkin et al., 2007) on Geneious using the default parameters and were color-coded by
589 similarity (Kearse et al., 2012).

590

591 **AlphaFold2 modelling of PKHD1L1 proteins.**

592 AlphaFold2 modelling was used to predict the structure of the mouse (*Mm)* PKHD1L1 protein region
593 comprising the residues p.3011-4249, harboring the potential cleavage sites and the antibody epitope of NBP2-
594 13765 (p.3670-p.3739). The protein sequence for the *Mm* PKHD1L1 protein fragment is reported in
595 supplementary table S1. AlphaFold2 simulation was carried out using the ColabFold v1.5.2-patch server using
596 default parameters (Mirdita et al., 2022). Figures were rendered using the VMD software (Humphrey et al.,
597 1996).

Acknowledgments

We would like to thank Dr. Jinwoong Bok for providing anti-STRC antibodies; Dr. Bradley Walters, Dr. Sumana Ghosh for RNAscope protocol and guidance. This work was supported by NIH R01DC020190 (NIDCD) and R01DC017166 (NIDCD) to A.A.I. and the Speech and Hearing Bioscience and Technology Program Training grant T32 DC000038 (NIDCD). The funders had no role in study design, data collection and analysis, decision to publish, or preparation of the manuscript.

Author contributions

OSS: Validation, Formal analysis, Investigation, Writing - Original Draft, Writing - Review & Editing, Visualization.
RTO: Formal analysis, Writing - Original Draft, Writing - Review & Editing, Visualization, Project administration.
CJT: Validation, Formal analysis, Investigation, Writing - Review & Editing
XYZ: Validation, Methodology, Formal analysis, Investigation, Resources, Writing - Review & Editing.
EH: Investigation, Writing - Review & Editing.
PD: Methodology, Validation, Formal analysis, Investigation, Writing - Review & Editing, Visualization.
DH: Methodology, Investigation, Writing - Review & Editing.
AAI: Conceptualization, Formal analysis, Investigation, Resources, Writing - Review & Editing, Supervision, Project administration, Funding acquisition.

References

Avan, P., Le Gal, S., Michel, V., Dupont, T., Hardelin, J. P., Petit, C., & Verpy, E. (2019). Otogelin, otogelin-like, and stereocilin form links connecting outer hair cell stereocilia to each other and the tectorial membrane. *Proceedings of the National Academy of Sciences of the United States of America*, *116*(51), 25948–25957. https://doi.org/10.1073/pnas.1902781116

Beurg, M., Fettiplace, R., Nam, J. H., & Ricci, A. J. (2009). Localization of inner hair cell mechanotransducer channels using high-speed calcium imaging. *Nature Neuroscience 2009 12:5*, *12*(5), 553–558. https://doi.org/10.1038/nn.2295

Chitre, A. S., Hebda-Bauer, E. K., Blandino, P., Bimschleger, H., Nguyen, K. M., Maras, P., Li, F., Ozel, A. B., Pan, Y., Polesskaya, O., Cheng, R., Flagel, S. B., Watson, S. J., Li, J., Akil, H., & Palmer, A. A. (2023). Genome-wide association study in a rat model of temperament identifies multiple loci for exploratory locomotion and anxiety-like traits. *Frontiers in Genetics*, *13*. https://doi.org/10.3389/FGENE.2022.1003074

Dolgobrodov, S. G., Lukashkin, A. N., & Russell, I. J. (2000a). *Electrostatic interaction between stereocilia: I. Its role in supporting the structure of the hair bundle*. www.elsevier.com/locate/heares

Dolgobrodov, S. G., Lukashkin, A. N., & Russell, I. J. (2000b). *Electrostatic interaction between stereocilia: II. Influence on the mechanical properties of the hair bundle*. www.elsevier.com/locate/heares

Duckert, P., Brunak, S., & Blom, N. (2004). Prediction of proprotein convertase cleavage sites. *Protein Engineering, Design and Selection*, *17*(1), 107–112. https://doi.org/10.1093/PROTEIN/GZH013

Fernandez, K. A., Guo, D., Micucci, S., De Gruttola, V., Liberman, M. C., & Kujawa, S. G. (2020). Noise-induced Cochlear Synaptopathy with and Without Sensory Cell Loss. *Neuroscience*, *427*, 43–57. https://doi.org/10.1016/j.neuroscience.2019.11.051

Fong, K. P., Barry, C., Tran, A. N., Traxler, E. A., Wannemacher, K. M., Tang, H. Y., Speicher, K. D., Blair, I. A., Speicher, D. W., Grosser, T., & Brass, L. F. (2011). Deciphering the human platelet sheddome. *Blood*, *117*(1). https://doi.org/10.1182/blood-2010-05-283838

Ghosh, S., Casey, G., Stansak, K. L., Thapa, P., & Walters, B. J. (2022). An Efficient Method to Detect Messenger RNA (mRNA) in the Inner Ear by RNAscope In Situ Hybridization. *Neuromethods*, *176*, 101–130. https://doi.org/10.1007/978-1-0716-2022-9_6/COVER

Goodyear, R. J., Cheatham, M. A., Naskar, S., Zhou, Y., Osgood, R. T., Zheng, J., & Richardson, G. P. (2019). Accelerated Age-Related Degradation of the Tectorial Membrane in the Ceacam16βgal/βgal Null Mutant Mouse, a Model for Late-Onset Human Hereditary Deafness DFNB113. *Frontiers in Molecular Neuroscience*, *12*. https://doi.org/10.3389/fnmol.2019.00147

Goodyear, R. J., Marcotti, W., Kros, C. J., & Richardson, G. P. (2005). Development and properties of stereociliary link types in hair cells of the mouse cochlea. *Journal of Comparative Neurology*, *485*(1), 75–85. https://doi.org/10.1002/cne.20513

Goodyear, R., & Richardson, G. P. (1999). The Ankle-Link Antigen: an Epitope Sensitive to Calcium Chelation Associated with the Hair-Cell Surface and the Calycal Processes of Photoreceptors. *Journal of Neuroscience*, *19*(10), 3761–3772. https://doi.org/10.1523/JNEUROSCI.19-10-03761.1999

Han, W., Shin, J.-O., Ma, J.-H., Min, H., Jung, J., Lee, J., Kim, U.-K., Choi, J. Y., Moon, S. J., Moon, D. W., Bok, J., & Kim, C. H. (2020). Distinct roles of stereociliary links in the nonlinear sound processing and noise resistance of cochlear outer hair cells. *Proceedings of the National Academy of Sciences*, *117*(20), 11109–11117. https://doi.org/10.1073/PNAS.1920229117

Humphrey, W., Dalke, A., & Schulten, K. (1996). VMD: Visual molecular dynamics. *Journal of Molecular Graphics*, *14*(1), 33–38. https://doi.org/10.1016/0263-7855(96)00018-5

Indzhykulian, A. A., Stepanyan, R., Nelina, A., Spinelli, K. J., Ahmed, Z. M., Belyantseva, I. A., Friedman, T. B., Barr-Gillespie, P. G., & Frolenkov, G. I. (2013). Molecular Remodeling of Tip Links Underlies Mechanosensory Regeneration in Auditory Hair Cells. *PLOS Biology*, *11*(6), e1001583. https://doi.org/10.1371/JOURNAL.PBIO.1001583

Ivanchenko, M. V., Indzhykulian, A. A., & Corey, D. P. (2021). Electron Microscopy Techniques for Investigating Structure and Composition of Hair-Cell Stereociliary Bundles. *Frontiers in Cell and Developmental Biology*, *9*, 744248. https://doi.org/10.3389/FCELL.2021.744248/BIBTEX

Jensen, J. B., Lysaght, A. C., Liberman, M. C., Qvortrup, K., & Stankovic, K. M. (2015). Immediate and Delayed Cochlear Neuropathy after Noise Exposure in Pubescent Mice. *PLOS ONE*, *10*(5), e0125160. https://doi.org/10.1371/JOURNAL.PONE.0125160

Kang, J. Y., Yang, J., Lee, H., Park, S., Gil, M., & Kim, K. E. (2023). Systematic Multiomic Analysis of PKHD1L1 Gene Expression and Its Role as a Predicting Biomarker for Immune Cell Infiltration in Skin

Cutaneous Melanoma and Lung Adenocarcinoma. *International Journal of Molecular Sciences*, *25*(1), 359. https://doi.org/10.3390/IJMS25010359

Karavitaki, K. D., & Corey, D. P. (2010). Sliding adhesion confers coherent motion to hair cell stereocilia and parallel gating to transduction channels. *Journal of Neuroscience*, *30*(27), 9051–9063. https://doi.org/10.1523/JNEUROSCI.4864-09.2010

Kazmierczak, P., Sakaguchi, H., Tokita, J., Wilson-Kubalek, E. M., Milligan, R. A., Müller, U., & Kachar, B. (2007). Cadherin 23 and protocadherin 15 interact to form tip-link filaments in sensory hair cells. *Nature*, *449*(7158), 87–91. https://doi.org/10.1038/nature06091

Kearse, M., Moir, R., Wilson, A., Stones-Havas, S., Cheung, M., Sturrock, S., Buxton, S., Cooper, A., Markowitz, S., Duran, C., Thierer, T., Ashton, B., Meintjes, P., & Drummond, A. (2012). Geneious Basic: An integrated and extendable desktop software platform for the organization and analysis of sequence data. *Bioinformatics*, *28*(12), 1647–1649. https://doi.org/10.1093/bioinformatics/bts199

Kujawa, S. G., & Liberman, M. C. (2006). Acceleration of age-related hearing loss by early noise exposure: Evidence of a misspent youth. *Journal of Neuroscience*, *26*(7), 2115–2123. https://doi.org/10.1523/JNEUROSCI.4985-05.2006

Kujawa, S. G., & Liberman, M. C. (2009). Adding insult to injury: Cochlear nerve degeneration after 'temporary' noise-induced hearing loss. *Journal of Neuroscience*, *29*(45), 14077–14085. https://doi.org/10.1523/JNEUROSCI.2845-09.2009

Larkin, M. A., Blackshields, G., Brown, N. P., Chenna, R., Mcgettigan, P. A., McWilliam, H., Valentin, F., Wallace, I. M., Wilm, A., Lopez, R., Thompson, J. D., Gibson, T. J., & Higgins, D. G. (2007). Clustal W and Clustal X version 2.0. *Bioinformatics*, *23*(21), 2947–2948. https://doi.org/10.1093/BIOINFORMATICS/BTM404

Legan, P. K., Lukashkina, V. A., Goodyear, R. J., Kössi, M., Russell, I. J., & Richardson, G. P. (2000). A targeted deletion in alpha-tectorin reveals that the tectorial membrane is required for the gain and timing of cochlear feedback. *Neuron*, *28*(1), 273–285. https://doi.org/10.1016/s0896-6273(00)00102-1

Legan, P. K., Lukashkina, V. A., Goodyear, R. J., Lukashkin, A. N., Verhoeven, K., Van Camp, G., Russell, I. J., & Richardson, G. P. (2005). A deafness mutation isolates a second role for the tectorial membrane in hearing. *Nature Neuroscience*, *8*(8), 1035–1042. https://doi.org/10.1038/nn1496

Lewis, M. A., Schulte, J., Matthews, L., Vaden, K. I., Steves, C. J., Williams, F. M. K., Schulte, B. A., Dubno, J. R., & Steel, K. P. (2023). Accurate phenotypic classification and exome sequencing allow identification of novel genes and variants associated with adult-onset hearing loss. *PLOS Genetics*, *19*(11), e1011058. https://doi.org/10.1371/JOURNAL.PGEN.1011058

Makrogkikas, S., Cheng, R. K., Lu, H., & Roy, S. (2023). A conserved function of Pkhd1l1, a mammalian hair cell stereociliary coat protein, in regulating hearing in zebrafish. *Journal of Neurogenetics*. https://doi.org/10.1080/01677063.2023.2187792

Matei, V., Pauley, S., Kaing, S., Rowitch, D., Beisel, K. W., Morris, K., Feng, F., Jones, K., Lee, J., & Fritzsch, B. (2005). Smaller inner ear sensory epithelia in Neurog1 null mice are related to earlier hair cell cycle exit. *Developmental Dynamics*, *234*(3), 633–650. https://doi.org/10.1002/DVDY.20551

Matern, M., Vijayakumar, S., Margulies, Z., Milon, B., Song, Y., Elkon, R., Zhang, X., Jones, S. M., & Hertzano, R. (2017). Gfi1Cre mice have early onset progressive hearing loss and induce recombination in numerous inner ear non-hair cells. *Scientific Reports*, *7*. https://doi.org/10.1038/srep42079

Michel, V., Goodyear, R. J., Weil, D., Marcotti, W., Perfettini, I., Wolfrum, U., Kros, C. J., Richardson, G. P., & Petit, C. (2005). Cadherin 23 is a component of the transient lateral links in the developing hair bundles of cochlear sensory cells. *Developmental Biology*, *280*(2), 281–294. https://doi.org/10.1016/J.YDBIO.2005.01.014

Mirdita, M., Schütze, K., Moriwaki, Y., Heo, L., Ovchinnikov, S., & Steinegger, M. (2022). ColabFold: making protein folding accessible to all. *Nature Methods*, *19*(6), 679–682. https://doi.org/10.1038/s41592-022-01488-1

Morisaki, N., Nakai, Y., Cho, H., & Shibata, S. (1991). Imprints of the tectorial membrane following acoustic overstimulation and kanamycin treatment. *Acta Oto-Laryngologica*, *111*(S486), 19–31. https://doi.org/10.3109/00016489109134978

Nayak, G. D., Ratnayaka, H. S. K., Goodyear, R. J., & Richardson, G. P. (2007). Development of the hair bundle and mechanotransduction. In *International Journal of Developmental Biology* (Vol. 51, Issues 6–7, pp. 597–608). https://doi.org/10.1387/ijdb.072392gn

Petit, C., & Richardson, G. P. (2009). Linking genes underlying deafness to hair-bundle development and function. In *Nature Neuroscience* (Vol. 12, Issue 6, pp. 703–710). https://doi.org/10.1038/nn.2330

Pickles, J. O., Comis, S. D., & Osborne, M. P. (1984). Cross-links between stereocilia in the guinea pig organ of Corti, and their possible relation to sensory transduction. *Hearing Research*, *15*(2), 103–112. https://doi.org/10.1016/0378-5955(84)90041-8

Redfield, S. E., De-la-Torre, P., Zamani, M., Khan, H., Morris, T., Shariati, G., Karimi, M., Kenna, M. A., Hun Seo, G., Naz, S., Indzhykulian, A. A., Eliot Shearer, A., & Vona, B. (n.d.). *PKHD1L1, A Gene Involved in the Stereociliary Coat, Causes Autosomal Recessive Nonsyndromic Hearing Loss 2 3*. https://doi.org/10.1101/2023.10.08.23296081

Richardson, G. P., & Petit, C. (2019). Hair-bundle links: Genetics as the gateway to function. *Cold Spring Harbor Perspectives in Medicine*, *9*(12). https://doi.org/10.1101/cshperspect.a033142

Ryan, A. F., Kujawa, S. G., Hammill, T., Le Prell, C., & Kil, J. (2016). Temporary and Permanent Noise-induced Threshold Shifts: A Review of Basic and Clinical Observations. *Otology and Neurotology*, *37*(8), e271–e275. https://doi.org/10.1097/MAO.0000000000001071

Santi, P. A., & Anderson, C. B. (1987). A newly identified surface coat on cochlear hair cells *. In *Hearing Research* (Vol. 21).

Saravia, C. H., Flores, C., Schwarz, L. J., Bravo, L., Zavaleta, J., Araujo, J., Neciosup, S., & Pinto, J. A. (2019). Patterns of Mutation Enrichment in Metastatic Triple-Negative Breast Cancer. *Clinical Medicine Insights. Oncology*, *13*. https://doi.org/10.1177/1179554919868482

Sellon, J. B., Ghaffari, R., & Freeman, D. M. (2019). The Tectorial Membrane: Mechanical Properties and Functions. *Cold Spring Harbor Perspectives in Medicine*, *9*(10), a033514. https://doi.org/10.1101/CSHPERSPECT.A033514

Shang, B., Yang, R., Lian, K., Dong, L., Liu, H., Wang, T., Yang, G., Xi, K., Xu, X., & Cheng, Y. (2024). Family-based genetic analysis in schizophrenia by whole-exome sequence to identify rare pathogenic variants. *American Journal of Medical Genetics. Part B, Neuropsychiatric Genetics : The Official Publication of the International Society of Psychiatric Genetics*. https://doi.org/10.1002/AJMG.B.32968

Song, D., Lyu, H., Feng, Q., Luo, J., Li, L., & Wang, X. (2021). Subtyping of head and neck squamous cell cancers based on immune signatures. *International Immunopharmacology*, *99*. https://doi.org/10.1016/J.INTIMP.2021.108007

Stringer, C., Wang, T., Michaelos, M., & Pachitariu, M. (2021). Cellpose: a generalist algorithm for cellular segmentation. *Nature Methods*, *18*(1), 100–106. https://doi.org/10.1038/s41592-020-01018-x

Suthakar, K., & Liberman, M. C. (2019). A simple algorithm for objective threshold determination of auditory brainstem responses. *Hearing Research*, *381*. https://doi.org/10.1016/j.heares.2019.107782

Verpy, E., Leibovici, M., Michalski, N., Goodyear, R. J., Houdon, C., Weil, D., Richardson, G. P., & Petit, C. (2011). Stereocilin connects outer hair cell stereocilia to one another and to the tectorial membrane. *Journal of Comparative Neurology*, *519*(2), 194–210. https://doi.org/10.1002/cne.22509

Verpy, E., Weil, D., Leibovici, M., Goodyear, R. J., Hamard, G., Houdon, C., Lefèvre, G. M., Hardelin, J. P., Richardson, G. P., Avan, P., & Petit, C. (2008). Stereocilin-deficient mice reveal the origin of cochlear waveform distortions. *Nature*, *456*(7219), 255. https://doi.org/10.1038/NATURE07380

Wang, L., Chen, Q., Liu, T., Bai, T., Zhang, M., Hu, Y., Li, J., & Chang, F. (2023). Role and mechanism of benzo[a]pyrene in the transformation of chronic obstructive pulmonary disease into lung adenocarcinoma. *Journal of Cancer Research and Clinical Oncology*, *149*(8), 4741–4760. https://doi.org/10.1007/S00432-022-04353-Y

Wang, Y., Hirose, K., & Liberman, M. C. (2002). Dynamics of Noise-Induced Cellular Injury and Repair in the Mouse Cochlea. *JARO: Journal of the Association for Research in Otolaryngology*, *3*(3), 248. https://doi.org/10.1007/S101620020028

Wu, X., Ivanchenko, M. V., Al Jandal, H., Cicconet, M., Indzhykulian, A. A., & Corey, D. P. (2019). PKHD1L1 is a coat protein of hair-cell stereocilia and is required for normal hearing. *Nature Communications*, *10*(1). https://doi.org/10.1038/s41467-019-11712-w

Yang, Y., Pang, Q., Hua, M., Huangfu, Z., Yan, R., Liu, W., Zhang, W., Shi, X., Xu, Y., & Shi, J. (2023). Excavation of diagnostic biomarkers and construction of prognostic model for clear cell renal cell carcinoma based on urine proteomics. *Frontiers in Oncology*, *13*. https://doi.org/10.3389/FONC.2023.1170567

Zheng, C., Quan, R., Xia, E. J., Bhandari, A., & Zhang, X. (2019). Original tumour suppressor gene polycystic kidney and hepatic disease 1-like 1 is associated with thyroid cancer cell progression. *Oncology Letters*, *18*(3), 3227–3235. https://doi.org/10.3892/OL.2019.10632

Zou, S., Ye, M., Zhang, J. an, Ji, H., Chen, Y., & Zhu, X. (2022). Establishment and genetically characterization of patient-derived xenograft models of cervical cancer. *BMC Medical Genomics*, *15*(1). https://doi.org/10.1186/S12920-022-01342-5

792 **Supplemental materials**

793

794

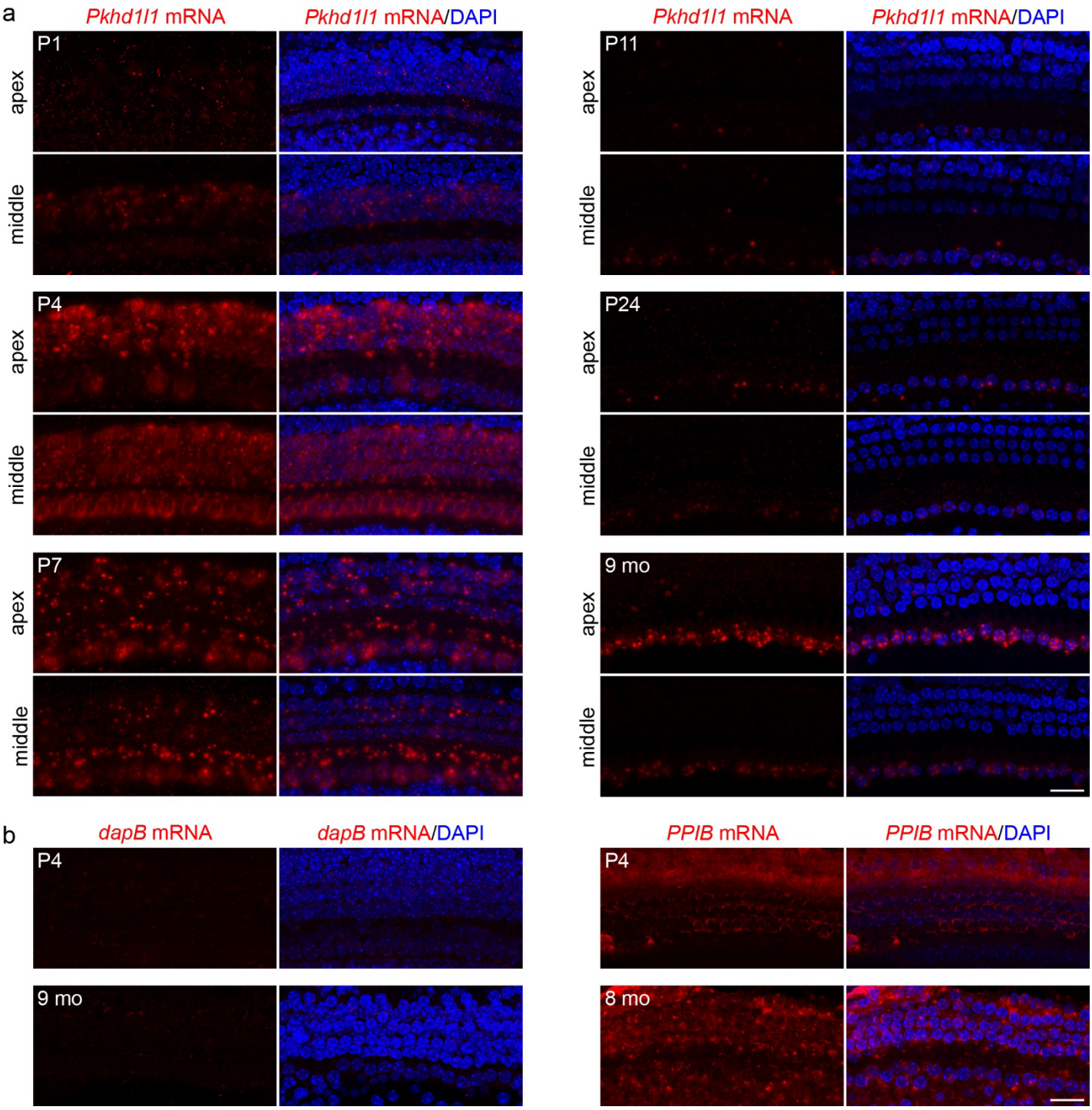

Supplemental Figure 1. *Pkhd1l1* mRNA levels in apical and mid-cochlear hair cells gradually decrease during early postnatal development. a, *In situ* detection of *Pkhd1l1* mRNA by RNAscope fluorescence labeling of the apical and mid-cochlear region reveals gradual decrease of mRNA signal in both, OHCs and IHCs by P11, while the mRNA levels in IHCs increase by 9 months. *Red*, *Pkhd1l1* mRNA fluorescence. *Blue*, DAPI. **b,** Negative control: *dapB* mRNA detection (dihydrodipicolinate reductase gene of *Bacillus subtilis*) in the mid-cochlear region shows negligible signal at P4 and 9-month time points. Positive control: *PPIB* mRNA (Cyclophilin B, ubiquitously expressed at low levels providing a rigorous control for sample quality) is detected at comparable levels in the mid-region of P4 and 8-month cochlea. *Scale bars,* 20 μm.

795

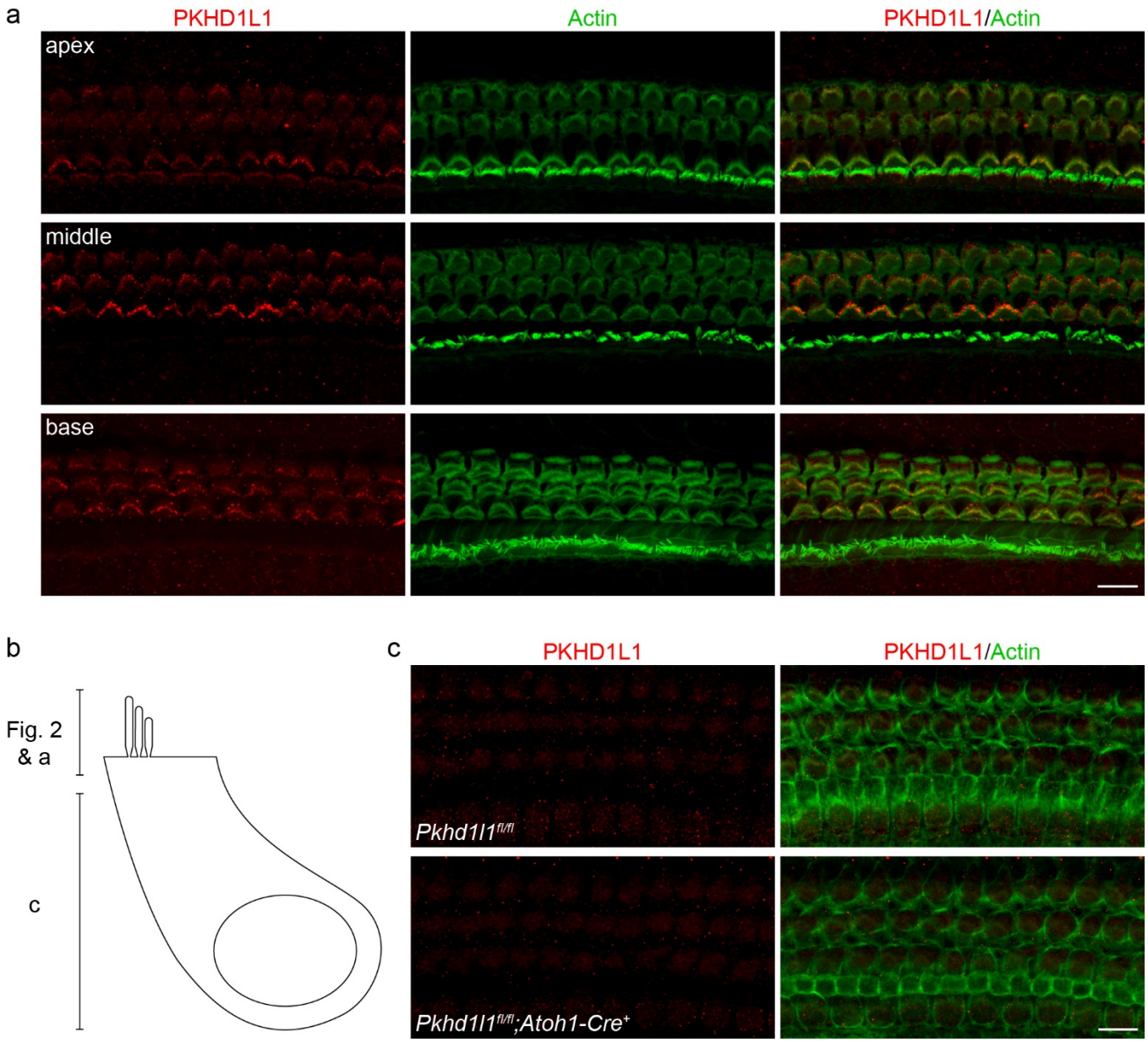

Supplemental Figure 2. **PKHD1L1 is primarily detected within hair-cell stereocilia bundles and not in cell bodies.**
a, Maximum intensity z-projection images of anti-PKHD1L1 labeling present in the hair cell stereocilia at P8 in the apex, middle and basal regions of the cochlea. **b,** Schematic of confocal z-projection depths in Figure 2 and panels a & c. **c,** Maximum intensity z-projection images of anti-PKHD1L1 labeling within the hair cell bodies at P4 in the basal region of the cochlea. No PKHD1L1-specific fluorescence is observed in normal *Pkhd1l1*$^{fl/fl}$*::Atoh1-Cre*$^{-}$ mice compared to *Pkhd1l1*$^{fl/fl}$*::Atoh1-Cre*$^{+}$ negative controls, although some non-specific labeling is present in both genotypes. *Red*, anti-PKHD1L1; *Green*, Phalloidin labeling. *Scale bars,* 10 µm.

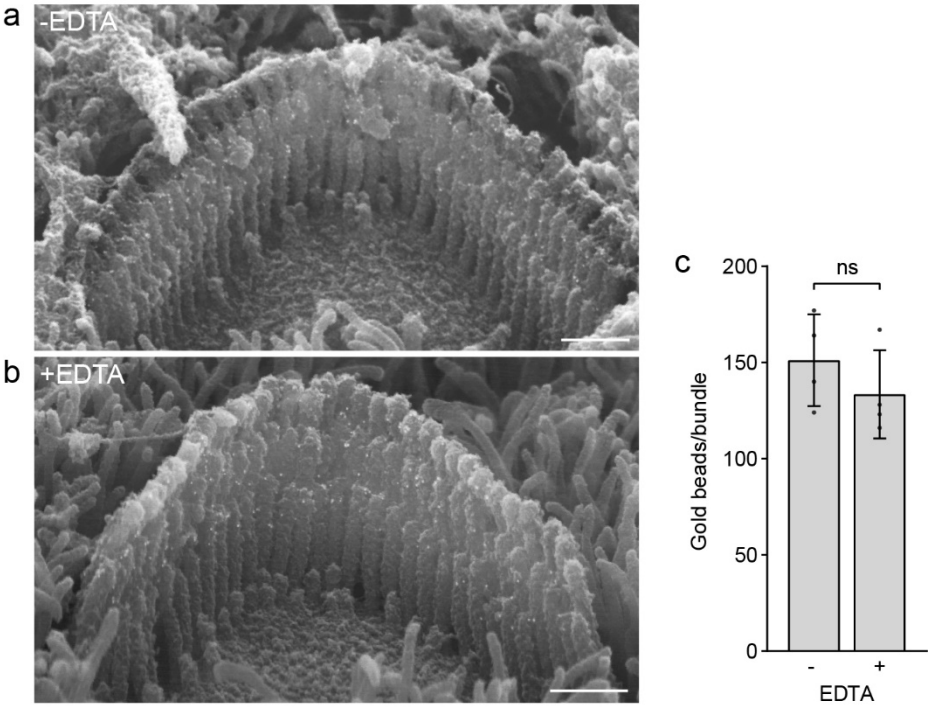

Supplemental Figure 3. **Anti-PKHD1L1 immunogold labeling efficiency is not affected by decalcification.**
a, Representative SEM images of OHC stereocilia bundle labeling of acutely fixed (*top*) and fixed then decalcified (*bottom*) cochlea. *Scale bar*, 500 nm. **b**, Quantification of gold beads per OHC stereocilia bundle. *Statistical analysis*, two-tailed t-test, p>0.05. Data displayed as mean ± SD, points represent individual cells (n=4 in each condition).

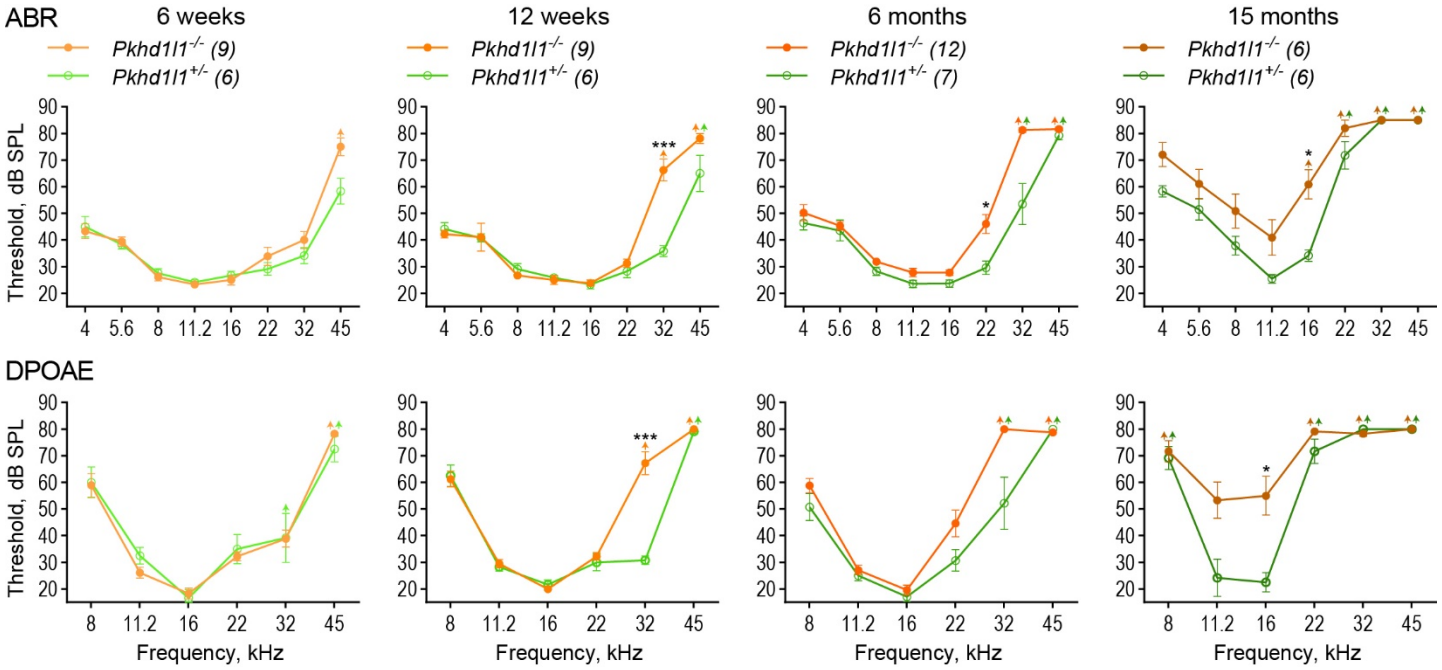

Supplemental Figure 4. *Pkhd1l1*$^{-/-}$ KO mice display progressive hearing loss.
ABR and DPOAE thresholds of constitutive *Pkhd1l1*$^{-/-}$ KO and *Pkhd1l1*$^{+/-}$ control littermate mice show progressive high-frequency hearing loss in PKHD1L1-deficient mice as early as 6 weeks. Data are shown as mean ± SEM. Up-arrows indicate that at the highest SPL level tested (80 dB SPL), at least one mouse in the group had no detectable thresholds at that frequency. *Statistical analysis*, two-way ANOVA with matched design between frequencies from the same mouse. Sidak's multiple comparison tests are shown between genotypes for each frequency. *p<0.05, **p<0.01, ***p<0.001.

797

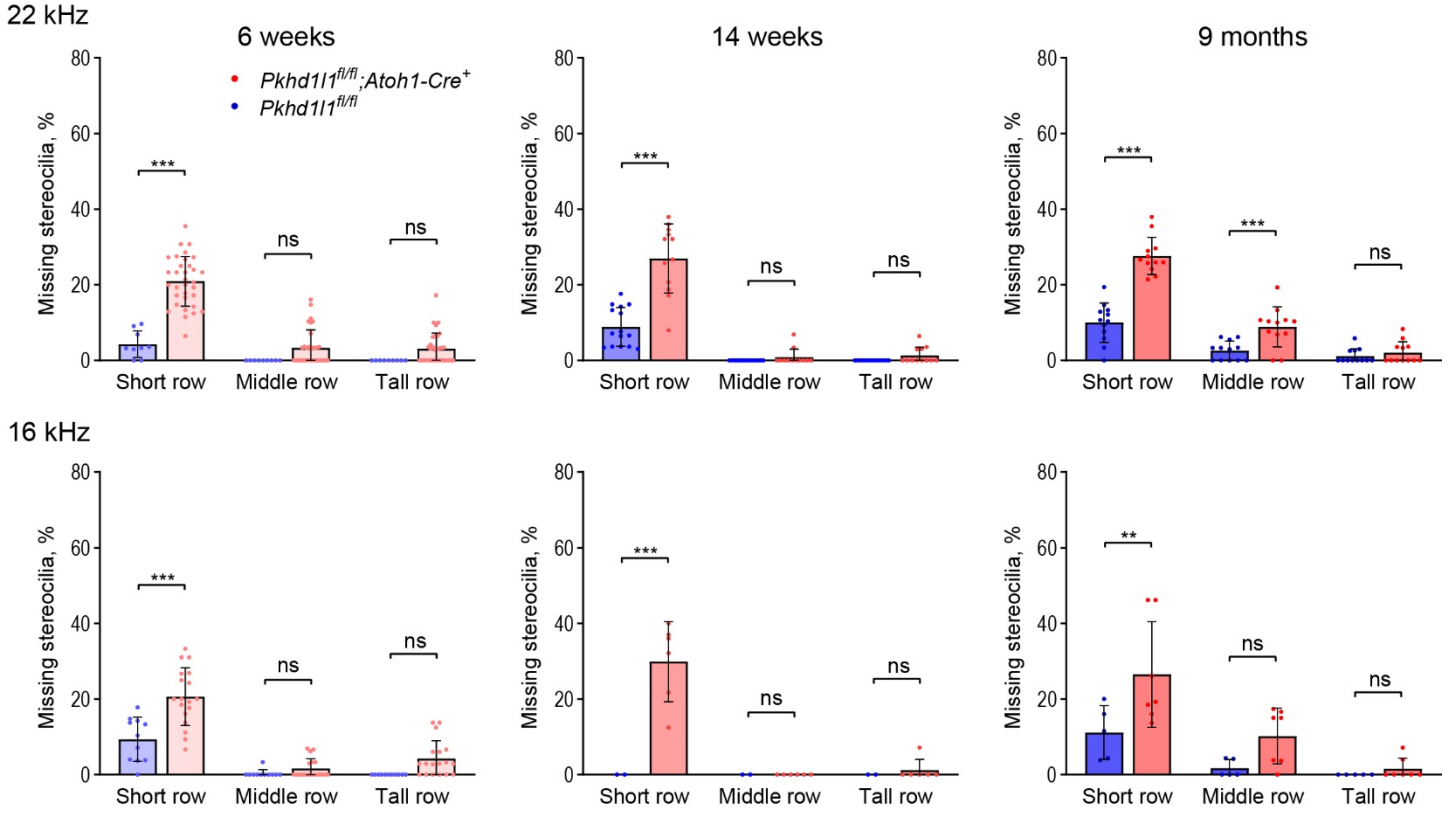

Supplemental Figure 5. Stereocilia loss in middle and apical regions of the cochlea of PKHD1L1-difficient mice. Quantification of missing stereocilia in OHC bundles in the 22 kHz (middle) and more apical, 16 kHz, regions of the cochlea, presented as percentage of missing stereocilia, per row. There is a greater stereocilia loss in *Pkhd1l1*$^{fl/fl}$*::Atoh1-Cre*$^{+}$ mice as compared to their *Pkhd1l1*$^{fl/fl}$*::Atoh1-Cre*$^{-}$ littermates at all age points. Data displayed as mean ± SD, points represent individual cells (n numbers in methods section). *Statistical analysis*, two-way ANOVA with matched design between rows from the same cell. Sidak's multiple comparison tests are shown between rows for each genotype. *p<0.05, **p<0.01, ***p<0.001.

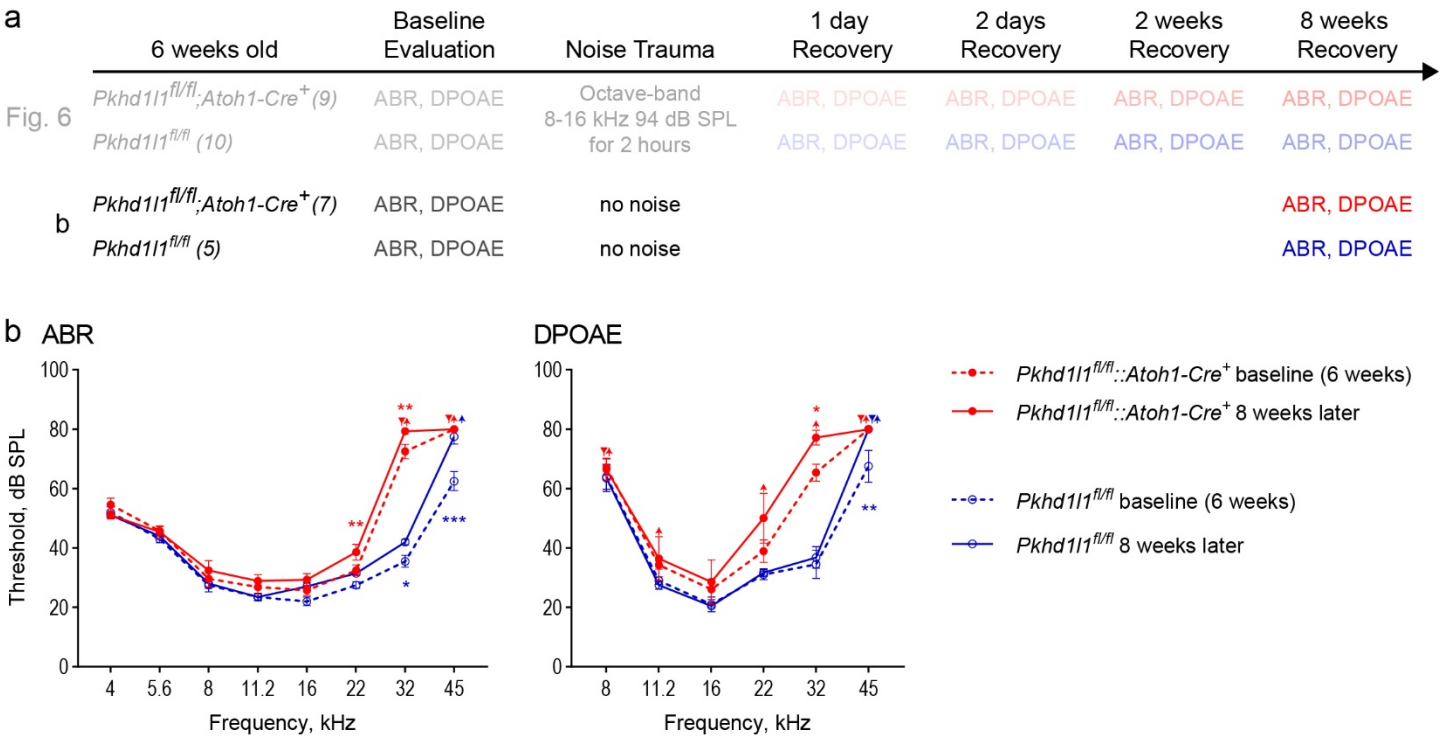

Supplemental Figure 6. Hearing performance of control mice that underwent no noise trauma exhibit detectable levels of progressive hearing loss 8 weeks later. a, Noise exposure experimental design with no noise controls. 6 week old *Pkhd1l1*$^{fl/fl}$*::Atoh1-Cre*$^{+}$ mice and *Pkhd1l1*$^{fl/fl}$*::Atoh1-Cre*$^{-}$ normal mice had baseline ABR and DPOAE evaluation prior to TTS-inducing level of noise trauma (Figure 6), or no noise trauma in controls (b). ABR and DPOAEs were recorded again 8 weeks later. **b**, ABR and DPOAE thresholds in no noise groups at 6 weeks (*dotted lines*) and 8 weeks later (*solid lines*). Both *Pkhd1l1*$^{fl/fl}$*::Atoh1-Cre*$^{-}$ control mice (*blue*) and *Pkhd1l1*$^{fl/fl}$*::Atoh1-Cre*$^{+}$ mice (*red*) show an increase in high frequency thresholds as a result of aging, in addition to the raised thresholds demonstrated in PKHD1L1-deficient mice. Data are shown as mean ± SEM. Inverted triangle (baseline) and up-arrows (8 weeks later) indicate that at the highest SPL level tested (80 dB SPL), at least one mouse in the group had no detectable thresholds at that frequency. *Statistical analysis*, two-way ANOVA with matched design between frequencies from the same mouse, and repeated measures at multiple time points. Sidak's multiple comparison tests are shown between time points for each frequency for both genotypes. *p<0.05, **p<0.01, ***p<0.001.

Table S1. Species and PKHD1L1 accession numbers used for multiple sequence alignment analysis, cleavage site prediction, and AlphaFold2 modelling.

Species	Abbreviation	NCBI Accession number
Homo sapiens	*Hs*	NP_803875.2
Mus musculus	*Mm*	NP_619615.2
Pan troglodytes	*Pt*	XP_016815270.3
Macaca mulatta	*Mm2*	XP_015001362.2
Otolemur garnettii	*Og*	XP_023373972.1
Sus scrofa	*Ss*	XP_020944671.1
Canis lupus familiaris	*Clf*	XP_038540795.1
Bos taurus	*Bt*	XP_024857633.1
Mustela lutreola	*Ml*	XP_059021749.1
Danio rerio	*Dr*	NP_001305057.1

799

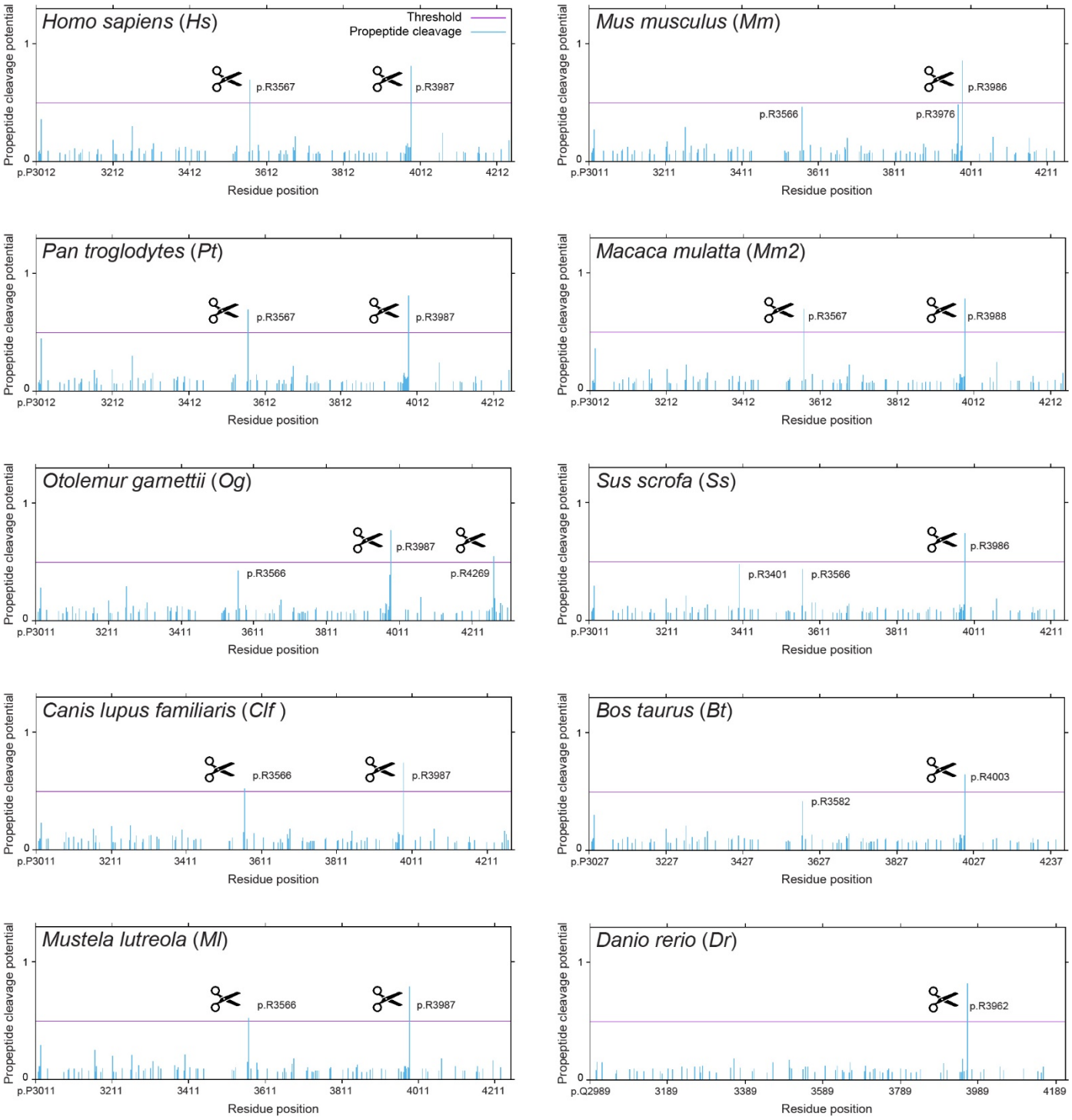

Supplemental Figure 7. Prediction of potential cleavage sites in PKHD1L1 proteins orthologs.
Cleavage sites were predicted across 10 different orthologs for full-length PKHD1L1 protein sequences. Only the region of each PKHD1L1 protein sequence where the cleavage sites are predicted are shown for clarity (see Sup. Table 1 for list of the species and NCBI accession codes). PKHD1L1 protein sequences were analyzed using the ProP v.1.0b ProPeptide Cleavage Site Prediction online server tool. The residue position is indicated for each species, based on NCBI accession numbers (Sup. Table S1) (X axes) and the score for each arginine (R) and lysine (K) residue is shown for the analyzed sequences (Y axes). A score of >0.5 (represented by the purple threshold line) was used to identify residues predicted to be a pro-peptide cleavage site (marked by a black scissor sign). Other plausible cleavage sites below the threshold line are also indicated by residue numbering. A higher score reflects a higher prediction confidence.